Distribution, style, amount of collisional shortening, and their link to Barrovian metamorphism in the European Alps

Claudio L. Rosenberg, Nicolas Bellahsen, Alain Rabaute, Jean-Baptiste Girault

Earth-Science Reviews xxx (xxxx) 103774

Contents lists available at ScienceDirect

Earth-Science Reviews

journal homepage: www.elsevier.com/locate/earscirev

Distribution, style, amount of collisional shortening, and their link to Barrovian metamorphism in the European Alps

C.L. Rosenberg *, N. Bellahsen, A. Rabaute

ISTeP, Institut des Sciences de la Terre de Paris, Sorbonne Université, 4 place Jussieu, 75005 Paris, France

ABSTRACT

We review estimates of collisional shortening along the Alpine Chain and reassess its amounts, showing that it increases from south to north in the Western Alps, attaining a maximum in the Central Alps, and decreasing in the Eastern Alps. We suggest that previous calculations overestimated shortening in the Western Alps, but underestimated it in the Central Alps. Based on these new determinations, we conclude that the convergence direction during Alpine collision was more likely oriented NW instead of WNW. A new map compilation of peak metamorphic temperatures related to *syn*-collisional, Barrovian metamorphism and of cooling ages for the Western Alps form the base for a discussion and interpretation of the spatial distribution of Barrow-type metamorphism throughout the Alpine Chain. We show that a simple correlation exists between the inferred temperature of areas where Barrow-type metamorphism is exposed at the surface and the amount of collisional shortening, which is mainly localized in the External Zone in the Western Alps, but in the Internal Zone in the Central and Eastern Alps. We conclude with a conceptual model, suggesting that major differences in the spatial distribution of shortening and exhumation of Barrovian metamorphic units across the Alpine Chain depend on the convergence direction, but also on the presence and size of the Briançonnais continental nappe stack at the onset of collision.

1. Introduction

Mature collisional orogens are characterized by the formation and exhumation of Barrow-type metamorphic terrains, as observed in numerous examples throughout the Phanerozoic (Caledonides, Appalachians, Hercynian belt, Himalayas, European Alps, Southern Alps of New Zealand). The occurrence of Barrow-type metamorphism in the Alps (e.g., Ernst, 1973; Frey et al., 1974; Niggli et al., 1978), and in particular in the Lepontine Dome of the western Central Alps (Fig. 1a, b), has been the subject of a long-standing debate on the timing and geodynamic cause of the heat sources of metamorphism. Whereas Wenk (1975) considered that Barrow-metamorphism was largely late-tectonic, due to a temperature dome associated with crustal melts, Niggli (1970) recognized the link between collision, hence stacking of nappes and their slow heating, following orogenic burial (Niggli, 1986 for review), thus assessing the Cenozoic age of Barrow-type metamorphism. Analytical thermal models (Oxburgh and Turcotte, 1974) stressed the importance of additional heat contribution from the mantle and the effect of erosion rates (England and Richardson, 1979; England, 1978) in order to explain the development of this *HT* metamorphism in the Tauern Dome (Fig. 1b). Indeed, several later models (Ridley, 1989; Huerta et al., 1996; 1998; Jamieson et al., 1998) showed that temperatures determined from mineral parageneses in Barrow-type terrains as those of the Alps cannot be explained without adding extra heat sources to the equilibrated thermal state of the crust that follows subduction. Numerical models of collision need to include radiogenic crustal material into the lower crust or mantle, thus avoiding its erosion and redistribution, in order to increase the heat budget of the collisional prism to a degree that is consistent with *T* and *P* conditions inferred from natural mineral parageneses (Jamieson et al., 1998). This idea was adapted to the specific geological setting of the Central Alps (Engi et al., 2001), where radiogenic crustal material was inferred to be accreted as a channel along the plate interface. Berger et al. (2011) showed that the *T* distribution of the Lepontine dome, as determined from mineral parageneses, depends both on the effect of advective heat, transported by the stacking of *HP* fragments, and by shortening of lower plate basement units, thus thickening and increasing the amount of radiogenic material in the orogenic wedge. Alternatively, viscous shear heating in the mantle (Burg and Gerya, 2005), and attenuation of the mantle lithosphere (Stüwe and Sandiford, 1995), were also suggested and modelled to be viable heat sources, respectively for the Lepontine metamorphism in the Central Alps and for the Tauern metamorphism in the Eastern Alps (Fig. 1).

Although Barrovian metamorphism typically develops during the collisional stages of orogeny, its distribution in the Alpine Chain is discontinuous along strike (Fig. 1b). Its amphibolite facies overprint is limited to the cores of the Lepontine and the Tauern domes (Fig. 1b; Ernst, 1971; Bousquet et al., 2012a, 2012b) and its greenschist facies overprint occurs in the peripheral zones of these domes in addition to the external part of the Western Alps. Metamorphism in the remaining

* Corresponding author.
E-mail address: claudio.rosenberg@sorbonne-universite.fr (C.L. Rosenberg).

https://doi.org/10.1016/j.earscirev.2021.103774
Received 6 March 2021; Received in revised form 12 August 2021; Accepted 13 August 2021
0012-8252/

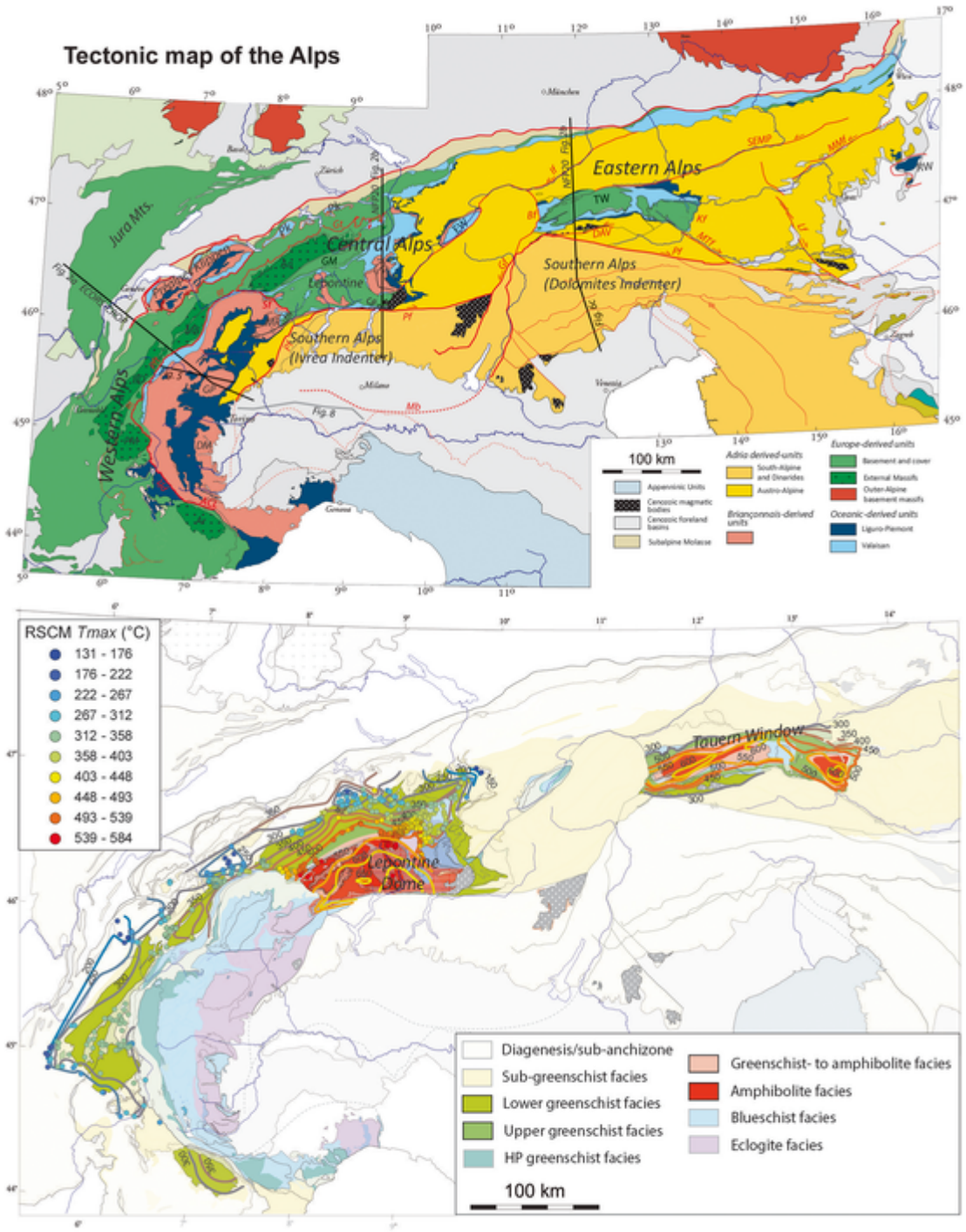

Fig. 1. a Simplified tectonic map of the Alps, modified from Bousquet et al. (2012a) showing the main paleogeographic domains. External Crystalline Massifs: *Aa*: Aar Massif; *Ar*: Argentera Massif; *BD*: Belledonne Massif; *MB*: Mt. Blanc Massif; *PM*: Pelvoux Massif. Internal Massifs: *GM*: Gotthard Massif; *GP*: Gran Paradiso; *MR*: Monte Rosa. Windows and Klippen: TW: Tauern Window; RW: Rechnitz Windows; *Pk*: Penninic Klippen. Faults: *ACL*: Acceglio-Cuneo-Lanzo Fault; *Bf*: Brenner Fault; *DAV*: Defereggen-Antholz-Vals Fault; *Gf*: Giudicarie Fault; *GT*: Glarus Thrust; *If*: Inntal Fault; *Kf*: Katschberg Fault; *Lt*: Lavantal Fault; *MB*: Milan Belt; *Mf*: Mür-Mürz Fault; *MTf*: Mölltal Fault; *PFt*: Penninic Front; *Pf*: Periadriatic Fault; *Rf*: Rhine- Fault; *Rt*: Roselend thrust; *SEMP*: Salzach-Ennstal-Mariazell-Puchberg Fault; *Folds*: *Va*: Vanzone antiform; *Ca*: Cressim antiform.

b. Map of Cenozoic Alpine metamorphism. Compiled iso-*T* contours of *syn*-collisional metamorphism along the Alpine Chain. Iso-*T* contours in the External Zone of the Western Alps and Aar and Gotthard massifs are based on RSCM data, interpolated using a classical near-neighbour algorithm. RSCM *T* are colour coded in 45 °C intervals. Iso-*T* lines in Lepontine and Tauern domes are taken respectively from Engi et al. (2004) and Rosenberg et al. (2018). Iso-*T* lines in the Argentera Massif are based on thermochronological data by Bigot-Cormier et al. (2000) and Corsini et al. (2004). Iso-*T* line in the Internal Zone is inferred on the base of thermochronological data of Fig. 3. RSCM data are compiled from: Bellanger et al. (2015), Berger et al. (2020), Boutoux et al. (2016), Gabalda et al. (2009), Girault et al. (2020), Girault et al. (2021), Mair et al. (2018), Negro et al. (2013), Nibourel et al. (2018), Nibourel et al. (2018), Wiederkehr et al. (2011). Metamorphic map of the Alps modified from Bousquet et al. (2012b).

parts of the Chain is either of pre-Alpine age (i.e. Variscan or Cretaceous), as in the overwhelming majority of the Adriatic nappes (Fig. 1a), or it is a pressure-dominated metamorphism resulting from Paleocene to Eocene subduction, as in the arc of the Western Alps and in the Engadine Window (Fig. 1a). Goffé et al. (2003) proposed that these differences in the *P-T* conditions of metamorphism along the strike of the Alps are largely controlled by lithological differences of the accreted crustal rocks. The highly radiogenic granodioritic compositions of the nappe stacks in the Lepontine and Tauern domes (Fig. 1a), in contrast to the low radiogenic meta-sediments between them, would explain the observed lateral gradients of metamorphic *T*. However, this interpretation is in conflict with orogen-scale cross sections of the Central Alps, which do not show a fundamental change in the lithological nature of the collisional prism across the boundary of the Lepontine dome (e.g., Rosenberg and Kissling, 2013). East of the Lepontine dome, tectonic units exposed at the surface and inferred to continue at depth (Rosenberg and Kissling, 2013) consist of lithologies typical for continental basements, similar to those of the Lepontine dome.

The above described along-strike variations, make the attempt to determine a general, unique and representative process of Alpine collision very difficult, even though the Alpine Chain is a text-book example for collisional orogens (e.g., Twiss and Moores, 1992; Moores and Twiss, 1995; Fossen, 2010; Johnson and Harley, 2012). It is the aim of the present study to reassess the amounts and the spatial distribution of collisional shortening all along the Alpine Belt.

2. Geologic setting

The Alpine Chain results from subduction of the Liguro-Piemont and Valais oceans, and the Briançonnais continental slice, followed by collision between the European and the Adriatic Plates (e.g., Laubscher, 1988; Roure et al., 1989; Nicolas et al., 1990; Stampfli, 1993; Froitzheim et al., 1996; Schlunegger and Kissling, 2015). Based on cross-sections and their retro-deformation, the process of collision in the Alps can be simply described as a sequence of crustal nappes detaching from the down-going continental mantle and lower crust, thus becoming accreted and eventually folded into a collisional prism (e.g., Argand, 1916; Laubscher, 1970; Milnes, 1978; Schmid et al., 1996). To a lesser degree, this process also affects the upper plate of the orogen, where tectonic transport was directed southward, hence in the opposite direction compared to the lower plate, making the Alps a bivergent orogen (Argand, 1916). For detailed and modern descriptions of the tectonic evolution of the Alps during Alpine subduction and collision, the reader is referred to Froitzheim et al. (1996), Handy et al. (2010), Stüwe and Schuster (2010), Le Breton et al. (2021). The description of the Alpine geologic setting below only focuses on Alpine collision and in particular on along-strike changes of collisional style and metamorphic facies. We define Alpine collision, as the accommodation of convergence after subduction of the distal and thinned European margin. Collision shortened the already existing nappe stacks in the internal parts of the orogen and created new nappes in the external part. The initiation of collision is inferred to coincide with Molasse sedimentation in the foreland basin, which is dated at 34–32 Ma (Sissingh, 1997).

For the sake of clarity, we will use the terms Western, Central, and Eastern Alps (Fig. 1a), when assessing amounts of collisional shortening. The Western Alps are located west and south of the Simplon Fault (Fig. 1a), the Central Alps are located between the Simplon and the Brenner faults (Fig. 1a), and the Eastern Alps are located east of the latter fault.

The nappes of the Alpine orogenic wedge are inferred to derive from five distinct paleogeographic domains (Fig. 1a). From top to bottom in cross-sectional view (Fig. 2) these domains are the Adriatic continental plate, the Liguro-Piemont oceanic domain, the Briançonnais continental domain, the Valais oceanic domain, and finally the European Plate. The Adria-derived units consist of Austroalpine and Southern Alpine,

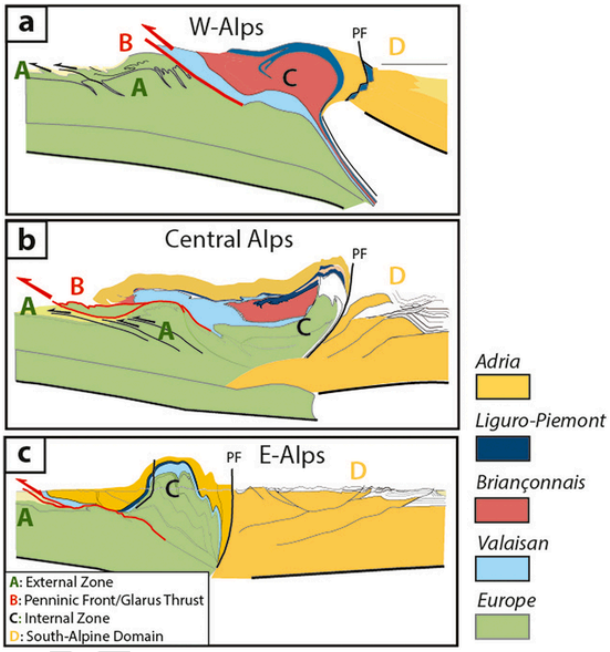

Fig. 2. Simplified sections based on integrated geological and seismic cross sections showing the 1st order structures, discussed in the text, which accommodated collisional shortening. Shortening estimates for each of these structures are discussed in the text. Traces of sections are shown in Fig. 1a. a) Western Alps, ECORS section, modified after Schmid et al., 2017; b) Central Alps, NFP20 SECTION, modified from Schmid et al. (1996) and Rosenberg and Kissling (2013); c) Eastern Alps, TRANSALP section, modified from Rosenberg et al. (2015).

with the Austroalpine nappes inferred to have occupied a more distal position in Jurassic Time. The Briançonnais nappes are derived from a continental slice, which bordered the Liguro-Piemont Ocean to its southeast and the Valais domain to its northwest. The Briançonnais nappes, together with those derived from both oceanic plates, form the Penninic domain in the Alps, which is also referred to as the Internal Zone, as opposed to the External Zone, which consists of Europe-derived units. Generally, the structurally deeper these units are located within the orogenic prism, the more external (to the northwest) their paleogeographic position was, before the onset of Alpine orogeny.

The Briançonnais nappes are exposed over most of the surface of the Internal Zone of the Western Alps, but they entirely disappear in the Eastern Alps (Fig. 1a). The thickness of the Briançonnais nappe stack progressively thins eastward. Whereas it attains approximately 25 km thickness in the Western Alps (e.g., Schmid et al., 2017) it is only 10 km thick in the NW Alps (Ecors section; Figs. 1a and 2a), 10 km thick in the Central Alps (Fig. 2b), and entirely absent in the Eastern Alps (Fig. 2c). The easternmost exposure of Briançonnais nappes in map view is in the Engadine Window (Fig. 1a), where their bulk thickness is reduced to only 5 km. Two reasons were proposed for the absence of Briançonnais in the Eastern Alps (Froitzheim et al., 1996): the first is of paleogeographic nature, suggesting that the eastern termination of Briançonnais nappes at the surface corresponds to the eastern termination of the Briançonnais continental domain before the onset of Alpine orogeny. The second suggests that the Briançonnais units in the Eastern Alps were not exhumed after subduction, hence not included in the orogenic wedge. Because of the continental nature of the Briançonnais domain, it is unlikely that no part of it was exhumed after subduction. Hence, the first interpretation above appears to be more likely.

The basement massifs of the Alps are classically distinguished into External (Argentera, Pelvoux, Belledonne, Aiguilles Rouges, Mont Blanc, Aar; Fig. 1a) and Internal Massifs (Dora Maira, Gran Paradiso, Monte Rosa; Fig. 1a). The difference clearly refers to their position with

respect to the foreland of the Alps. However, the Internal Massifs share a different geological Alpine history, because they consist of basement nappes that were subducted before the onset of collision, whereas the External Massifs consist of nappes that only formed during collision. In addition, the Internal Massifs consist of Briançonnais nappes, whereas the External Massifs consist of shortened and thickened portions of the European basement. In spite of its European basement core, we include the Tauern dome to the Internal Massifs, because it also consists of a stack of basement nappes that were affected by subduction-metamorphism, previous to doming and Barrow metamorphism during collision. In contrast, we include the Engadine Window to the External Massifs. Although the European Basement is not exposed there, it is inferred from seismic interpretations (Hitz, 1995) that the window forms on top of a pile of European basement nappes located in a rather external position of the orogen.

In the Western Alps the External and Internal Massifs are located in the External and Internal Zones, respectively (e.g., Debelmas and Kerckhove, 1980). The Internal Zone in the Western Alps is delimited eastward by the Austroalpine Units (but only by the Molasse sediments in the southern part of the arc; Fig. 1a). In the west it is delimited by the Penninic Front (Fig. 1a), a major thrust transporting the stack of subducted nappes derived from the Briançonnais, Valais, and Liguro-Piemont domains over the European paleo-margin.

The Periadriatic Fault (Fig. 1a), represents the northern limit of the Southalpine Indenters (Ivrea indenter in the west and Dolomites indenter in the east, Fig. 1a), which acted as back-stops during collision (Ratschbacher et al., 1991; Robl and Stüwe, 2005; Schmid et al., 2017). The rocks exposed at the surface within these indenters were not affected by Cenozoic Alpine metamorphism (Fig. 1b).

The inferred amount of collisional shortening varies along strike (Schönborn, 1992; Bellahsen et al., 2014; Rosenberg et al., 2015; Liao et al., 2018). Recent studies that estimated shortening between the Present and the time around initiation of collision suggest that in the Western Alps, shortening was inferred to amount to 124 km (Schmid and Kissling, 2000), but later reassessed to 243 km (Handy et al., 2010), or 227 km (Handy et al., 2015), if calculated along a N303°W direction. Schmid et al. (2017), in their paleogeographic reconstruction of the entire Alpine Realm, proposed that some 200 km of WNW–directed shortening affected the arc of the Western Alps after 35 Ma.

Post-32 Ma shortening across the Central and Southern Alps was inferred to be 119 km (Schmid et al., 1996). Changes of shortening along the strike of the orogen were shown to be small across the Central Alps, varying between 117 and 127 km (Rosenberg et al., 2015). However, none of the estimated values above is representative of bulk collisional convergence, because they do not include strike-slip displacements along the dextral Periadriatic Fault (Fig. 1a).

In the Eastern Alps, collisional shortening was estimated to be 420 km (Roeder, 1989), but later interpreted to be significantly less: Schönborn (1999) and Nussbaum (2000) calculated some 50 km of shortening south of the Periadriatic Fault, and Linzer et al. (2002) estimated between 61 and 64 km of shortening north of the Periadriatic Fault, thus providing bulk shortening estimates between 111 and 114 km. Alternatively, 149 km or 125 km were suggested, respectively, by Rosenberg and Berger (2009) and Favaro et al. (2017) for the westernmost part of the Eastern Alps. However, shortening north of the Periadriatic Fault was inferred to decrease from 75 km in the west to 30 km in the east (Rosenberg et al., 2018), possibly due to a clockwise rotation of the Dolomites Indenter (Bertrand et al., 2015; Rosenberg et al., 2015). This would decrease bulk collisional shortening from 125 km in the western- to 80 km in the eastern Eastern Alps.

In summary, previous reconstructions suggest that collisional shortening in the Western Alps is larger by a factor of 1.5 to 2, compared to the Central Alps and to the Eastern Alps, hence requiring a rather westward directed convergence during collision.

Cenozoic metamorphic rocks (arbitrarily defined as having reached $T > 250$ °C) crop out discontinuously along the Alpine orogen. The entire arc of the Western Alps and the western part of the Central Alps are formed by a Cenozoic metamorphic belt, which terminates at the boundary between Penninic and Austroalpine Units in the Central Alps (Fig. 1b; Bousquet et al., 2012a, 2012b). The eastern part of the Central Alps, from the latter boundary to the Brenner Fault, does not show any Cenozoic metamorphism, i.e. temperatures were ≤ 250 °C, as shown by the age of low-*T* thermo-chronological data (zircon FT; Fox et al., 2016) that are consistently older than 30 Ma. In the Western Alps, from the external to the most internal parts of the arc, a rather regular pattern of metamorphic facies can be traced (Ernst, 1971; Bousquet et al., 2012b; Fig. 1b), going from lower green-schist facies, to pressure-affected green-schist facies, to blue-schist facies and finally attaining eclogite facies. The boundaries between these metamorphic facies strike subparallel to the orogen. The Internal Zone is affected, in different units, by a retrograde greenschist facies metamorphism. In the Central Alps, the metamorphic zonation is different, because *HP* metamorphic rocks are largely overprinted by collision-related, Barrovian metamorphism (e.g., Todd and Engi, 1997; Wiederkehr et al., 2011; Bousquet et al., 2012b, for map-view distribution of metamorphic facies). Maximum *T* of over 700 °C and maximum *P* of 0.7 GPa are inferred to have been attained at 30 Ma (Berger et al., 2011). East of the Lepontine dome, where surface outcrops consist of Austroalpine Units, Cenozoic metamorphism is absent. In the Engadine Window, where Penninic Units are exposed, lower green-schist facies metamorphism is *syn*-collisional, based on thermo-chronological data (Evans, 2011, her Fig. 15), indicating that He in zircon ages were reset during Oligocene times within the Penninic Units.

The Eastern Alps do not show any Cenozoic metamorphic overprint except for the Tauern Window, the Rechnitz Windows, and a slice of Austroalpine Units bordering the southwestern corner of the Tauern Window (Borsi et al., 1973; Fig. 1b). Metamorphic conditions in the Tauern Window are also characterized by Barrow-type metamorphism overprinting a subduction-related mineral assemblages (Selverstone, 1988). Iso-*T* contours are sub-parallel to- and symmetrically distributed about the hinge of the Tauern Dome, forming an elongate concentric pattern with maximum *T* of 650 °C in the core of the western sub-dome (Hoernes and Friedrichsen, 1974) at pressures of~0.7 GPa (Selverstone, 1993), and 525 °C in the eastern sub-dome (Scharf et al., 2013). These peak *T* were most likely attained between 30 and 28 Ma (Cliff et al., 2015).

Both the Lepontine and the Tauern domes are bounded by syn-collisional normal faults (Behrmann, 1988; Selverstone, 1988; Mancktelow, 1990), which accommodated orogen-parallel extension, thus contributing to exhumation of these domes. The activity of these normal faults reduced the vertical thickness of the orogenic wedge, by accommodating orogen-parallel extension.

3. Syn-collisional Alpine metamorphism

Fig. 1b shows a new compilation of *T*-data used to visualise the patterns of syn-collisional, iso-*T* lines on the scale of the entire Alpine orogen. The data are mainly derived from petrologic and RSCM (Raman Spectrometry of Carbonaceous Material) analyses in areas where independent age determinations indicated post-32 Ma ages (Crouzet et al., 1999; Engi et al., 2004; Gabalda et al., 2009; Sanchez et al., 2011; Wiederkehr et al., 2011; Scharf et al., 2013; Bellanger et al., 2015; Boutoux et al., 2016; Nibourel et al., 2018; Girault et al., 2020). Thermo-chronological data (Malusà et al., 2005; Rolland et al., 2008; Sanchez et al., 2011; Wolff et al., 2012; Bellanger et al., 2015; Boutoux et al., 2016) providing both age and closure *T* are also included in the figure.

In addition to the well-known exposures of Barrow-type metamorphic assemblages in the Lepontine and Tauern domes, the compilation of Fig. 1b shows that Barrow-type metamorphism the arc affected the

arc of Western Alps, all along its external part, namely in the basement and cover units of the European margin. In this area iso-*T* contour lines are sub-parallel to the major collisional structures with maximum *T* located in the cores of the External Massifs, attaining a maximum of 450 °C in the Aar (Engi et al., 2004; Herwegh et al., 2020), 400 °C in the Mont Blanc (Rolland et al., 2003), and 350 °C in the Pelvoux and Argentera Massifs (Sanchez et al., 2011). In the Lepontine dome (Fig. 1b) a geothermal gradient between 22 °C in the southern Aar Massif (T = 525 °C, Nibourel et al., 2018; P = 0.65GPa; Goncalves et al., 2012) and 35 °C/km in the southeastern part of the dome can be assessed.

Where iso-*T* lines are mapped in detail it is clear that they cross cut major contacts between the nappes that were stacked during the transition from continental subduction to continental collision. This is well documented in the Tauern Window (Hoernes and Friedrichsen, 1974; Scharf et al., 2013; Rosenberg et al., 2018), in the Central Alps (Engi et al., 2004; Wiederkehr et al., 2011), and in the Western Alps (Girault et al., 2020).

4. Spatial distribution of cooling ages in the Western Alps

Fig. 4 presents a new compilation and interpolation of zircon fission track ages in map view. Their spatial distribution shows that the Internal Zone passed through the partial annealing zone ($T \sim 250$ °C) approximately at 30 Ma (as previously shown by Malusà et al., 2005, and Fox et al., 2016). These data are consistent with the inferred emplacement of the 31 Ma old Biella Pluton (Romer et al., 1996) at less than 7 km depth (Zanoni et al., 2008), but possibly even closer to the surface (Bigioggero and Tunesi, 1988), indicating that less than 7 km have been eroded since 31 Ma in the Internal Zone. Only in the northernmost part of the Internal Zone, in the vicinity of the Simplon normal fault, zircon fission track ages are younger, mostly Early Miocene (Fig. 3). Because the brittle-ductile transition of quartz under natural strain rate conditions is inferred to take place at ~275 °C (Stipp et al., 2002), it is inferred that the presently exposed Internal Zone of the Western Alps was already included into the brittle, upper crust at 30 Ma, hence at the beginning of collision.

If apatite fission track ages are plotted along an *E*-W section crossing the Gran Paradiso Massif (Malusà et al., 2005), they show a large scale, symmetric younging, forming a bell shape on an age vs distance dia-

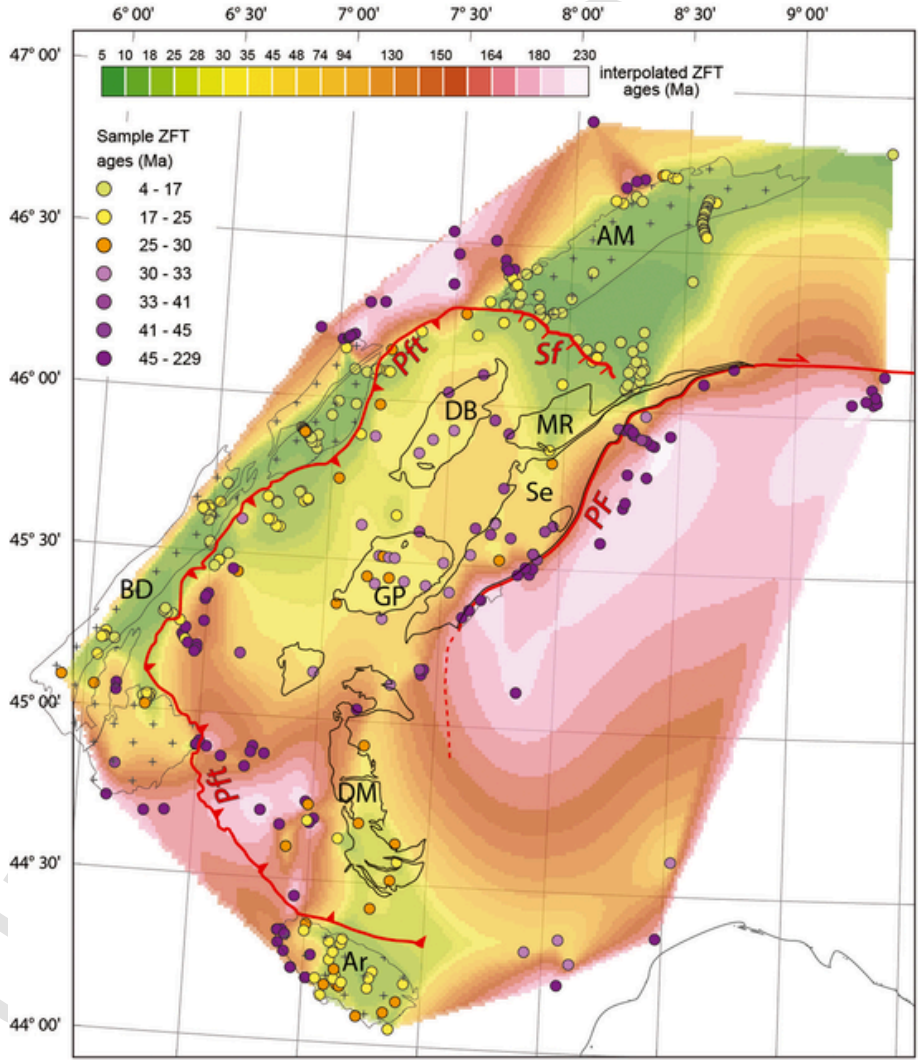

Fig. 3. Compiled and interpolated isoage contour lines from zircon fission tracks, throughout the Western Alps. Ar: Argentera Massif; BD: Belledonne; DB: Dent Blanche; DM: Dora Maira; GP: Gran Paradiso; MB: Mont Blanc; MR: Monte Rosa; Se: Sesia. *Pft*: Penninic front; *PF*: Periadriatic Fault; *Sf*: Simplon fault. Data are compiled from: Soom (1990); Hurford et al. (1991); Lelarge (1993); Seward and Mancktelow (1994); Sabil (1995); Vance (1999); Bigot-Cormier et al. (2000); Fügenschuh and Schmid (2003); Keller et al. (2005); Malusà et al. (2005); Schwartz et al. (2007); Siegesmund et al. (2008); Campani et al. (2010); van der Beek et al. (2010); Glotzbach et al. (2011); Sanchez et al. (2011); Girault et al. (2021).

gram (Fig. 4). This pattern is typical for areas exhumed by antiformal folding and erosion (Batt and Braun, 1997; Bertrand et al., 2015; Rosenberg et al., 2018). Ages vary from ~32 Ma at the margins to 12 Ma in the central area of the Internal Zone, which coincides with the hinge of the Gran Paradiso antiform. Therefore folding must have affected the Gran Paradiso Massif until 12 Ma. Alternatively, if the above fission track ages are inferred to represent re-equilibration of the isotherms after advective rock uplift during folding (e.g., Bertrand et al., 2013), their age postdates the folding event.

The fact that the bell shape only affects the apatite fission track ages but not the zircon ages (Fig. 4) suggests that the amplitude of folding, was small. Its associated exhumation was sufficient to reset apatite fission track ages but not the zircon ones. Therefore, collisional shortening accommodated by folding of the Internal Zone was not associated with significant amounts of shortening, which is consistent with the large ratio of wavelength (> 50 km) to amplitude (10 km) of the Gran Paradiso antiform.

The compilation and interpolation of zircon fission track ages of Fig. 3 shows older ages (≥ 30 Ma) in the hangingwall of the Penninic Front, and younger ones (Miocene) in its footwall. The separation between these age domains does not coincide exactly with the trace of the Penninic Front, but rather with a larger area of up to 10 km width in the hanging wall of the latter thrust (Fig. 3; Malusà et al., 2005, their Fig. 7; Fox et al., 2016), which accommodated thrusting of the Internal Zone.

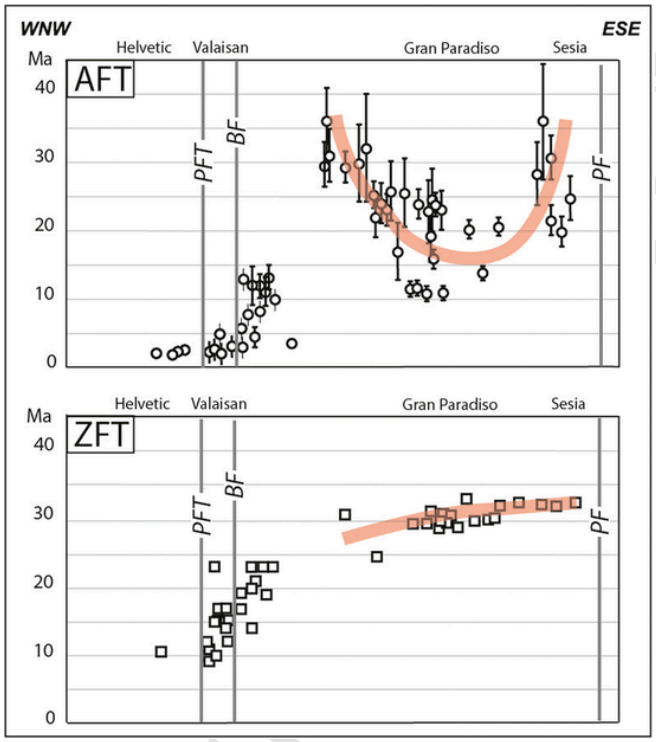

Fig. 4. Distance vs fission track age diagrams, across the Internal Zone of the Western Alps, modified from Malusà et al. (2005). Trace of the section crosses the Gran Paradiso Massif as shown in Fig. 1a.). AFT: Apatite fission tracks; ZFT: Zircon fission tracks. *BF*: Briançonnais Front; *PF*: Periadriatic Fault; *PFT*: Penninic Frontal Thrust; Closure *T* of apatite is 120 °C and closure *T* of zircon is 250 °C. Note the sub-horizontal trend of zircon ages at around 30 Ma across the Gran Paradiso antiformal structure, but the bell-shaped trend of the apatite fission track ages in the same area, with progressively younger ages towards the core of the antiform. This trend typically indicates cooling during folding and erosion, which however, did not affect the higher *T* system of zircon fission tracks.

5. Amount and distribution of collisional shortening: A re-assessment

Estimates of the amount of shortening accommodated in the Alpine orogen were provided since its structure was first recognized as the superposition of large-scale nappes. Termier (1903) suggested that up to 150 km of displacement were accommodated by displacement of the nappes. Heim (1908) considered that "*The Alps are … replacing a flat-lying continental zone of 600 to 1200 km width*". Argand (1916) inferred that the total amount of convergence between Adria and Europe was larger than 1000 km. However, his retro-deformation suggests that after the formation and stacking of the nappes in the Internal Zone, i.e. after subduction (as we conceive it nowadays), only few tens of km of shortening affected the orogen (Argand, 1916).

Even in more modern literature, attempts to quantify Alpine shortening remain very difficult, because in the internal parts of the chain appropriate sedimentary markers are generally missing. In the present study, we attempt to reassess the amount of *syn*-collisional shortening based on retro-deformation of the first-order collisional structures in the Western, Central, and Eastern Alps. For each of these three areas we define and describe below, with the help of three simplified cross sections (Fig. 2), which of the structures are of 1st order and need to be retro-deformed in order to quantify collisional shortening. Minor structures are inferred to be rooted in the latter ones and do not need to be taken into account.

In the Western Alps, we calculate shortening within four distinct domains. From the foreland to the internal part of the chain, these domains are (Fig. 2a): 1) the External Zone, comprising the basement and cover of the European margin, whose thrusts are rooted in the European basement (e.g., Bellahsen et al., 2014); 2) the Penninic Front, which forms the boundary between Valais-derived and Europe-derived nappes, and continues to be active during collision along the Roselend thrust segment (Ceriani et al., 2001); 3) the Internal Zone, consisting of Briançonnais and Liguro-Piemont nappes which is shortened by small amplitude and large wave-length folds, and by thrusts rooted in the Briançonnais basement; 4) the Southern Alps, whose minor shortening, if present, is rooted in the basement of the upper plate (Fig. 2a).

In the Central Alps, estimates of shortening can be similarly divided within four principal areas, as illustrated in Fig. 2b: 1) the External Zone, consisting of the Jura-fold-and-thrust-belt (Fig. 1a), as well as the Helvetic Nappes and their basement, which is formed by the Aar Massif; 2) the Glarus thrust and the Penninic Front. Based on the cross section of Schmid et al. (1996; their Plate I), these two thrusts coincide over a large distance, but the Glarus crosscuts the Penninic Front. The Glarus thrust is rooted south of the Aar Massif, in the European basement (Burkhard, 1990; Schmid et al., 1996; Pfiffner, 2011); 3) the Internal Zone, characterized by large-scale antiforms folding the Monte Rosa and Bergell Massifs (Vanzone and Cressim antiforms, respectively; Fig. 1a), and finally; 4) the upper plate, corresponding to the Southern Alps.

In the Eastern Alps, collisional shortening is accommodated by southward thrusting in the Southern Alps (Dolomites), by the large-scale antiformal structure of the Tauern Window north of the Periadriatic Fault, by the thrusts of the Subalpine Molasse, and by conjugate strike-slip faults, accommodating the eastward displacement of the orogenic wedge (Fig. 2c). The Basal Penninic Thrust, does not appear to be an active plane of displacement after the earliest Oligocene (e.g., Ortner et al., 2015), hence it is not taken into account to quantify shortening. The site within the European basement, where the thrusts of the Subalpine Molasse are rooted, is not fully constrained. One possibility is that they are kinematically connected to basement thrusts of the Tauern Window, hence at a distance of approximately 50 to 70 km from their surface exposure at the front of the orogen. Seismic sections do not show any other evidence of thrusting within basement units north of the Tauern Window, hence displacements accommodated in

the Subalpine Molasse may be taken into account by estimating shortening in the basement of the Tauern Window. We will discuss the two possibilities below.

5.1. Reassessing the amount of collisional shortening in the Western Alps

Table 1 is a summary of previous estimates of collisional shortening in the Western Alps. The paragraphs below describe how we recalculate bulk collisional shortening from the sum of shortening accommodated along all structures described in Fig. 2a.

5.1.1. External Zone

Shortening amounts are taken from restored cross sections (Burkhard, 1988; Burkhard and Sommaruga, 1998; Ford et al.; 2006; Bellahsen et al., 2014), which used offsets of sedimentary markers, where present (Mugnier et al., 1990), and balancing of the "excess surface" of the basement in other areas (External Massifs; Burkhard, 1988). As shown in Fig. 5, based on these data, collisional shortening increases from south to north, from 21 km in the Argentera Massif (Fig. 1a) section to 46 km in the Pelvoux (Fig. 1a) section, to 66 km in the northern Mont Blanc section (Fig. 5).

Table 1
Compilation of inferred amounts of collisional shortening in the Western Alps from previous literature.

Authors	Inferred amount and timing of shortening	Area and method used for estimating shortening
Beach, 1981	30 to 70 km in the External Zone	Restored section, between Penninic Front and western margin of Belledonne Massif, assuming constant cross-sectional area.
Butler, 1985	126 km in the External Zone	Restored section between external Belledonne Massif and Penninic Front
Butler, 1985	180 km in the External Zone	Restored section between external Pelvoux Massif and Penninic Front
Butler, 1985 (Butler et al., 1986)	385 km post-Late Eocene to Miocene	Restored section between Jura Front and Po Plain. Section striking across Gran Paradiso Massif
Lacassin, 1989	100–150 km in the External Zone	Beach 1981: restoration of section between External Massifs and Penninic Front
Laubscher, 1991	approximately 150 km post-Oligocene *E*-W shortening	Map-view restoration of the entire Alpine Chain
Mugnier et al., 1990	35 km – 50 km in the External Zone	Line length restoration of cross section from the Penninic Front to the Foreland Basin, across the Belledonne Massif
Schmid and Kissling, 2000	124 km: Post-35 Ma	Map-view restoration based on estimates of shortening in Central Alpine cross section from southern to northern Molasse basins and assumed dextral offset of 100 km along Periadriatic Fault
Handy et al., 2010	243 km, post 35 Ma *E*-W shortening	Extrapolation of shortening values from Central Alps. 63 km of N-S shortening north of the Periadriatic Fault, resolved on the assumed convergence direction (N303°W) that is based- on average orientation of stretching lineations in the W-Alps.
Handy et al., 2015	308 km, post-35 Ma	Retro-deformation of the entire Alpine Realm, assuming 180 km dextral strike-slip along the Periadriatic Fault
Bellahsen et al., 2014	27–28 km, post 33 Ma, in the External Zone	Balanced section, from the Molasse Basin, to the Penninic Front, across the Belledonne-Pelvoux area
Burkhard and Sommaruga, 1998	65.9 km post 30 Ma	Balanced section, from the Frontal Jura thrust, to the Penninic Front, across the Préalpes and Mt. Blanc
Schmid et al., 2017	~ 200 km post 35 Ma	Estimates inferred from restored cross sections and large-scale plate reconstructions

5.1.2. Penninic front

The Penninic Front (Fig. 1a) forms the boundary between the subduction-related metamorphic area of the western Alpine Arc (Penninic Domain) in its hangingwall and the External, Europe-derived Domain in its footwall (Fig. 1a). This large-scale thrust can be followed in map view from the northern part of the Argentera Massif to the Simplon Fault (Fig. 1) in the Western Alps. It has been imaged at depth along seismic reflection profiles (Ecors, Fig. 1a: Roure et al., 1990a, 1990b) and by P-wave receiver function studies (Zhao et al., 2015). Based on radiometric dating of its deformation fabrics, the Penninic Basal Thrust is inferred to be active at 38 Ma and to be reactivated as an out-of-sequence thrust at 27 Ma (Cardello et al., 2019). Cross-cutting relationships indicate that its activity post-dated the Priabonian deposits of its footwall. In some areas a footwall splay of the Penninic front, cuts through the European cover. It is termed the Roselend thrust (Ceriani et al., 2001), and it is inferred to be active in the Early Oligocene (Ceriani et al., 2001). This thrust represents the syn-collisional continuation of the Penninic Front, and as such it is difficult to estimate its offset and separate it from the one of the Penninic Front itself, which was active in the latest stages of subduction. The amount of syn-collisional displacement was constrained by considering that its top-to-the west displacement is accommodated along a dextral offset of the Penninic Front at its northern termination (Fig. 1a; Ceriani et al., 2001), and a sinistral strike-slip fault at its southern termination, (Ceriani et al., 2001; Molli et al., 2010; Schmid et al., 2017; Fig. 1). The former dextral fault is the Rhine-Fault (Fig. 1a) and the latter sinistral fault, striking north of the Argentera Massif (Fig. 5; Ceriani et al., 2001), is termed Acceglio-Cuneo Line (Schmid et al., 2017; Fig. 1a). The map-view offset accommodated by each of these faults is ~ 50 km (Fig. 5), hence the amount of top-to-the west displacement accommodated by the Roselend Thrust would also be of 50 km. However, strike-slip displacements along the aforementioned faults are speculative. First, because the *E*-W strike and apparent dextral offset of the Penninic Front is part of a large-scale bend in map view, in an area that is structurally lower compared to the Aar and Mt. Blanc Massifs on its both sides (Fig. 5). Hence, part of this bend is merely an effect of the intersection of the E-dip of the fault and the surface. The Acceglio-Cuneo Line (Fig. 1a) provides an apparent sinistral offset of the Penninic Front, however, no structural analysis of this inferred sinistral fault exists in the literature yet. For all these reasons, we consider the value of 50 km (Fig. 5) as an absolute maximum. Further north, in the area located north of the Mt. Blanc Massif, cross sections indicate that the Penninic Basal Thrust covers Oligocene sediments over a distance of 67 km (Cardello et al., 2019), or approximately 80 km (Burkhard and Sommaruga, 1998; their Fig. 6), which is therefore taken as the amount of syn-collisional displacement of the Penninic Front north of the Mt. Blanc Massif in Fig. 5.

5.1.3. Internal Zone

Collisional shortening within the Internal Zone is mainly accommodated by folding of the Gran Paradiso (Fig. 1a) and the other Internal Massifs (e.g., Bucher et al., 2004). In addition to structural arguments (Bucher et al., 2004), thermo-chronological data (Malusà et al., 2005) confirm that doming occurred during collision and that it was not related to large amounts of uplift and exhumation of the Massif itself (see discussion above in Section 4). We calculate by line-length balancing of this structure that it accommodated a maximum of 12 km of E-W shortening. Further south, in the area of the Dora Maira Massif, both exhumation ages and geometrical constraints in cross-section are scarce, but shortening does not seem to exceed that of the Gran Paradiso Massif. This small amount of collisional shortening in an area that was highly deformed during subduction, is consistent with the ages of low-*T* cooling systems, as zircon fission tracks (Fig. 4), which are mostly older than 30 Ma. This indicates that exhumation in the Internal Zone was not very significant during collision, as expected for an area undergoing modest shortening.

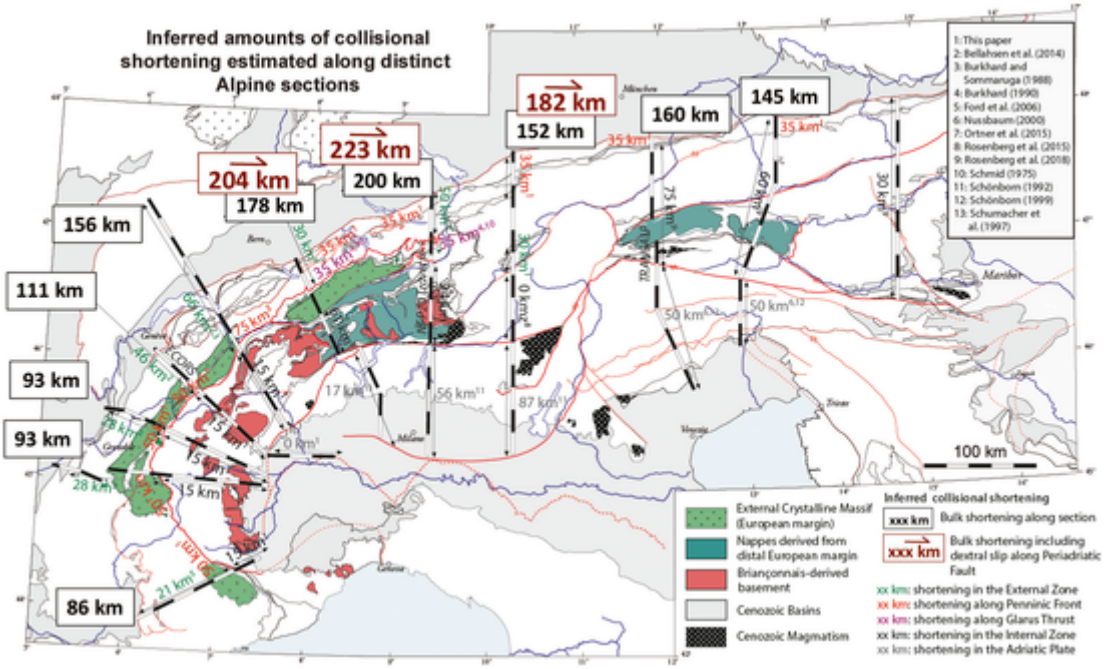

Fig. 5. Inferred amounts of *syn*-collisional shortening in map view. Tectonic map simplified after Bousquet et al. (2012b). Traces of sections along which shortening is estimated are shown. Different colours of the numbers refer to the different structures or domains shown in Fig. 2. Larger, black numbers within rectangle indicate bulk shortening representative of one section, whose trace is shown in the map. This value is calculated from the sum of individual amounts (numbers without rectangle) estimated for each segment of the section.

5.1.4. Southern Alps (upper plate)

The upper plate of the Western Alps is largely covered by Cenozoic Molasse deposits of the Po Basin. East-west striking seismic sections through this area (Pieri and Groppi, 1981; Fig. 6), illustrate a sequence of sub-horizontal Mesozoic and Cenozoic units that points to the absence of shortening during Cenozoic time. Hence, shortening west of the Periadriatic Fault represents the bulk of Alpine shortening during collision in the Western Alps.

Summing up the estimates above we conclude that maximum values of collisional shortening in the Western Alps (Fig. 5) varied from 86 km in the south (Argentera section) to 156 km in the North (Mont Blanc section).

5.2. Reassessing the amount of collisional shortening in the Central Alps (between Simplon and Giudicarie Faults)

A compilation of literature data on the inferred amounts of shortening in the Central Alps is presented in Table 2. These data mostly derive from studies along the NFP20 traverse (Fig. 1a, b), which is the one with best structural and geophysical constraints. Shortening amounts vary significantly along strike in the Central and Southern Alps (Schönborn, 1992; Rosenberg and Kissling, 2013) as shown in Fig. 5 and briefly discussed in our reassessment below. The areas and structures whose retro-deformation is discussed below are illustrated in Fig. 2.

5.2.1. Subalpine Molasse/Aar Massif

The Subalpine Molasse accommodated some 50 km of shortening, based on retro-deformation of balanced sections (Ortner et al., 2015; Pomella et al., 2015) located approximately 25 km east the of NFP20 Traverse (Fig. 1a). This displacement is inferred to be rooted within basement thrusts in the Aar Massif (e.g. Burkhard, 1990; Ortner et al., 2015). Previous studies calculated 21 km of shortening in the Aar Massif along the NFP20 traverse (Schmid et al., 1996; Rosenberg and Kissling, 2013) based on line-length balancing of the basement-cover surface of the Massif. The latter is, however, reconstructed mainly by lateral projections, because the European basement is only barely exposed along the NFP20 traverse (Fig. 1a). Assuming that the 50 km shortening assessed by balancing offsets of the sedimentary markers in the subalpine Molasse (Ortner et al., 2015) are a more robust estimate compared to line-length balancing of the Aar Massif, and that the Subalpine Molasse thrusts are rooted in the Aar Massif, we take the value of 50 km as representative of the amount of shortening in the latter areas for the NFP20 traverse. For sections located further east, striking across the Engadine Window, we take the value of 25 km, also based on balancing sections of the Subalpine Molasse (Ortner et al., 2015).

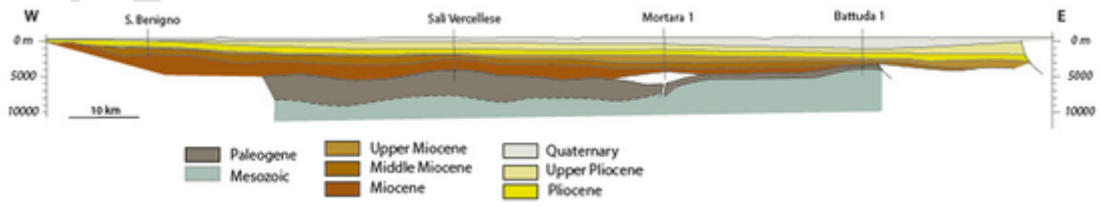

Fig. 6. Interpreted, E-W striking seismic section across the Western Alps. Modified after Pieri and Groppi (1981). The flat-lying reflectors, corresponding to flat-lying stratigraphic units, suggest that no shortening was accommodated within the Adriatic crust in this area, throughout Cenozoic times. Trace of section is shown as gray line in Fig. 1a.

Table 2
Compilation of literature data on inferred amounts of collisional shortening in the Central Alps, along the NFP20 section (Fig. 2b).

Authors	Inferred amount and timing of N-S shortening	Area and method used for estimating shortening
Hsu, 1979	100 km post-Eocene shortening	Restoration of cross sections between Periadriatic Fault and northern Alpine Front
Lacassin, 1989	65 km shortening north of Periadriatic Fault.	Based on 150 km shortening estimate along a N120°E direction in the W-Alps and a rigid plate model limited by dextral-slip along the E-W striking Periadriatic Fault
Laubscher, 1991	200 km, post Eocene shortening	Map-view restorations of 100 km shortening inferred to be 35 to 16 My old and additional 100 km post 16 Ma.
Schönborn, 1992	From E to W: 56 km, post Oligocene shortening in the Southern Alps	Restored balanced cross sections, between Periadriatic Fault and Milan Belt.
Schmid et al., 1996	125 km of post-Eocene shortening	Restoration of cross section, between Milan Belt and northern Alpine Front
Rosenberg and Kissling, 2013	From E to W: 12 km, 42 km, and 71 km, post Eocene shortening, north of Periadriatic Fault.	Restoration of cross sections and compilation of previous data, between Periadriatic Fault and northern Alpine Front, not including dextral displacement along the latter fault.
Rosenberg et al., 2015	From E to W: 30 km, 71 km, 95 km.	Restoration of cross sections and compilation of previous data between Periadriatic Fault and northern Alpine Front
Handy et al., 2015	151 km, Late-Eocene and post-Eocene shortening	Summing up values from Pfiffner (2009) for Helvetic Nappes and Schönborn (1992) for Southern Alps, between Periadriatic Fault and Milan Belt
Schmid et al., 2017	115 km, European crust	Within European crust, based on area balance on cross sections, assuming decoupling along the interface between upper and lower crust

Along the westernmost section of the Central Alps, crossing the western Aar Massif (Fig. 5), shortening amounts derived from balanced section of the Subalpine Molasse and Jura Mts (Fig. 1a) are inferred to lie between 25 and 30 km (Burkhard, 1990). Shortening in this area is accommodated by thrusts that root within the Aar Massif (Burkhard, 1990). Line-length balancing of the western Aar Massif was inferred to correlate with an amount of 34 km of shortening (Rosenberg et al., 2015). Therefore, for the Aar Massif/Subalpine Molasse/Jura Mts area we take an average shortening amount of 30 km (Fig. 5).

Along the easternmost section of the Central Alps (Fig. 5), striking across the Engadine Window, no External Massif is exposed. However, the antiformal structure building the Engadine Window is inferred to be the uppermost part of a basement antiformal stack, as indicated by seismic reflectors (Hitz, 1995). The latter structure was inferred to accommodate 10–12 km of shortening based on line-length balancing of a folded surface in the seismic section (Hitz, 1995). However, if the inferred basement thrusts (Hitz, 1995) are retro-deformed, larger amounts of shortening are required, namely around 30 km. Larger amounts of shortening are also coherent with the unusually large thickness of the Valaisan Unit in the Engadine Window (see section in Rosenberg and Kissling, 2013).

5.2.2. Glarus thrust

The Glarus thrust (Fig. 1a; Fig. 2) accommodated some 30–40 km of displacement (Schmid, 1975) since the Lower Oligocene (Hunziker, 1987; Burkhard, 1990; Schmid et al., 1996; Schmid et al., 1997), and it is rooted south of the External Aar Massif, namely between the Aar Massif and the Gotthard Massif (Fig. 1a; e.g. Schmid et al., 1996; Pfiffner, 2011). Therefore, its displacement must be added to the one of the Subalpine Molasse, which itself is rooted within the Aar Massif (e.g., Burkhard, 1988), when calculating bulk collisional shortening.

5.2.3. Penninic front

The Penninic Front in the Central Alps is rarely taken into consideration when retro-deforming collisional shortening. Pfiffner (2014) considered that the Penninic Front is no longer active in post-Eocene time, but Burkhard (1988) pointed out that its activity continues during the Grindelwald phase, which is of Oligocene age. Schmid et al. (1996) also suggested that the Pennine Front continues its displacement during the Pizol phase, which is Early Oligocene. Thrusting of South Helvetic and Ultrahelvetic flysch units above the Helvetic nappes is inferred to result from displacement of the Penninic Front on top of the Flysch Units during the Early Oligocene (Schmid et al., 1996). Moreover, the lateral continuity between the Penninic Préalpes Klippen and the smaller Penninic Klippen further east (Fig. 1a), only interrupted in map view by erosion, invokes relatively similar amounts of displacement of the Penninic Front at the same time over the entire area, which covers the transition between Western and Central Alps.

Based on the cross section of Schmid et al. (1996; their Plate I) the amount of displacement accommodated by the Penninic Front between the southernmost Aar Massif and the northern Alpine Front is similar to that inferred further west by Burkhard and Sommaruga (1998). However, one part of this thrust coincides with the Glarus thrust, which is inferred to accommodate 30–40 km of displacement. Thus, in order to avoid duplicating the amount of calculated displacement, *syn*-collisional shortening accommodated by the Penninic Front in the Central Alps is taken as 75 km (calculated from the section of Burkhard and Sommaruga, 1998) minus the amount of displacement along the Glarus thrust (40 km, taking the larger displacement mentioned above), hence 35 km (Fig. 5).

5.2.4. Cressim and Vanzone antiforms

The Cressim Antiform (Fig. 1a) folds the Adula/Gruf nappes and the Bergell Pluton on top of them. It is inferred to be coeval with emplacement of the Bergell Pluton (Rosenberg et al., 1995), which is dated at 31.5–28 Ma (Oberli et al., 2004), hence providing a good time constraint on shortening. This fold is possibly the lateral continuation of the Vanzone Antiform (Fig. 1a) in the western Central Alps, which folds the Monte Rosa nappe. Based on line-length restoration (Rosenberg and Kissling, 2013), simply assuming no thickening of the fold hinge, the Vanzone antiform accommodated 37 km of shortening, and the Cressim 24 km. However, the amplitude, hence the amount of shortening, of the Cressim antiform gradually decreases eastward and totally disappears east of the Liguro-Piemont ophiolites, east of the Bergell Pluton (Figs. 1 and 5; Spillmann, 1993). Hence, no collisional shortening is detected in the latter area along the easternmost section of the Central Alps (Fig. 5).

5.2.5. Southern Alpine thrusts

Along the NFP20 traverse (Fig. 1a), 56 km of post-Eocene shortening were accommodated in the Southern Alps, based on retro-deformation of balanced cross sections (Fig. 5; Schönborn, 1992). However, shortening increases to 87 km further east (Fig. 5; Schönborn, 1992), and decreases to 17 km further west (Fig. 5; Schumacher et al., 1997).

5.2.6. Periadriatic fault

The amount of *syn*-collisional dextral strike-slip accommodated along the Periadriatic Fault is poorly constrained, and interpretations provide values varying between a maximum of 150 to 180 km (Laubscher, 1991; Handy et al., 2015; respectively) and a minimum of 50 km (Müller et al., 2001), or even less, based on paleogeomorphological arguments (Garzanti and Malusà, 2008). The absolute value of this offset needs to be taken into account when calculating bulk collisional convergence accommodated in the Southern and Central Alps.

If an intermediate value of 100 km dextral displacement is considered (e.g., Schmid and Kissling, 2000) and a rigid-block model includ-

ing Southern Alps and Central Alps is assumed (Lacassin, 1989; Schmid and Kissling, 2000), a vector addition including north-oriented shortening of the Central Alps (200 km; Fig. 5), and *E*-W oriented dextral offset of 100 km along the Periadriatic Fault yields a maximum shortening of 223 km, along a N150°E direction in the central part of the Central Alps (NFP20 Traverse; Fig. 5). This value decreases to 204 km in the west, and to 182 km to the east (Fig. 5). If smaller and larger amounts of dextral strike-slip are assumed, taking a minimum value of 50 km and a maximum of 150 km, bulk convergence in the central Central Alps would correspond respectively to 206 and 250 km.

The estimates described above, do not take into account orogen-parallel extension, mainly localized along the Simplon Fault (Fig. 1a), which forms the western boundary of the Central Alps. Extensional, fault-parallel displacement is inferred to have attained 18–30 km (Campani et al., 2010). This displacement drives part of the collisional wedge laterally, in orogen-parallel direction, thus out of the cross section used to calculate shortening in the western Central Alps (Fig. 5). Therefore the calculated amount of horizontal shortening may be underestimated there.

5.3. Reassessing the amount of collisional shortening in the Eastern Alps

The areas and structures, whose retro-deformation is discussed below, are illustrated in Fig. 2c.

5.3.1. Subalpine Molasse

Shortening within the Subalpine Molasse decreases eastward, from 50 to 0 km, respectively, between 10° and 13° longitude (Fig. 1a; Ortner et al., 2015), with values of approximately 10 km, north of the western Tauern Window (Fig. 5). If these subalpine thrusts are rooted in the European basement north of the Tauern Window, their displacement needs to be added to the one inferred above for the Tauern Window and the Austroalpine nappes surrounding it, in order to obtain the bulk amount of shortening north of the Periadriatic Fault. Instead, if these thrusts are in kinematic continuity with the basal thrusts of the Tauern Window, their displacement does not need to be added to the one calculated already for the area north of the Periadriatic Fault. Based on present-day seismic interpretations along the TRANSALP traverse (Gebrande and TRANSALP Working Group, 2002; Kummerow et al., 2004; Figs. 1a and 2c), no significant basement thrusts are inferred to exist north of the Tauern Window (e.g., Ortner, 2006), consistently with the absence of External Massifs in this part of the Alpine Belt. Therefore, although the distance between the Subalpine Molasse and the basement thrusts of the Tauern Window is larger than 60 km, it is likely that displacements were continuously transferred from the former to the latter. We opt for this interpretation in Fig. 5, and do not add shortening of the Subalpine Molasse to our calculation. Note, however, that the absolute value of shortening in the Subalpine Molasse is inferred to be around 10 km only in the area north of the Tauern Window (Ortner et al., 2015), but such relatively small amount of shortening may not be so obviously detected from seismic interpretations.

At the onset of collision, the frontal part of the Eastern Alps were also affected by shortening due to displacement of the Helvetic nappes on top of the Molasse Basin (Lower Oligocene; Ortner et al., 2015). We have no markers to assess the amount of Early Oligocene displacement on this thrust, but by analogy with the Glarus thrust exposed further west we attribute 35 km to this displacement (Fig. 5).

5.3.2. Strike-slip faulting and upright folding north of the Periadriatic Fault

Large-scale, conjugate strike-slip faults, affected the Eastern Alps between the Northern Calcareous Alps and the Periadriatic Fault (Linzer et al., 2002; Fig. 1a) during collision (Ratschbacher et al., 1991; Bartosch et al., 2017). Retro-deformation of strike-slip displacements in map view results in 75 km of N-S shortening in the western Tauern Window and only 30 km east of the Window (Rosenberg et al., 2018). These displacements include dextral strike-slip along the Periadriatic Fault, which is therefore not considered separately, as for the Central Alpine area.

As discussed in Rosenberg et al. (2018) shortening of the Tauern antiformal structure (50 km; Rosenberg et al., 2015) is kinematically linked with the strike slip faults mentioned above. It accommodates large part of the 75 km of N-S shortening and does not need to be additionally taken into account when calculating bulk shortening of the orogen. In other words, lateral extrusion along eastward-diverging strike-slip faults displaces material eastward, and this “loss” is compensated by N-S shortening in the Tauern Window.

5.3.3. Southern Alps

Based on several N-S oriented balanced cross sections, both Schönborn (1999) and Nussbaum (2000) suggested that 50 km of shortening were accommodated in a series of ENE striking, south-vergent Miocene thrusts. This value is consistent with the more conservative amount of 30 km assessed by Doglioni (1992), limited to the southern segment of the Southern Alps. Along-strike variations in the amount of shortening are not observed (Nussbaum, 2000).

6. Relationship between shortening and *syn*-collisional metamorphic temperature in the Alpine Basement Massifs

In order to test if a simple relationship between the amount of collisional shortening and the *T* of collisional metamorphism in rocks exposed at the surface exists, we compiled and re-calculated shortening percentages of all basement massifs (Fig. 7). Due to the lack of appropriate markers, the calculation of shortening in the basement massifs is difficult, and different techniques leading to different results have been used in previous literature. For the external Massifs of the Western Alps, shortening in the basement was inferred by calculating displacements of thrusts crossing the lower Triassic (not detached from the basement) and folding of the Triassic attesting for internal basement deformation. Because these thrusts are rooted in the basement massifs, their displacement values are inferred to represent shortening of both the External Massifs and their cover (e.g., Bellahsen et al., 2014). Alternatively, shortening was assessed by assuming the depth of detachment of thrusts below the basement massifs (e.g., Burkhard and Sommaruga, 1998) and by balancing the surface area of displaced material in cross section. Finally, line-length balancing of the basement/cover interface was also used to estimate shortening in some of the External Massifs (e.g., Schmid et al., 1996; Schmid et al., 2013; Rosenberg and Kissling, 2013; Bellahsen et al., 2014; Rosenberg et al., 2015). The latter technique does not need an assumption on the detachment depth, but it may severely underestimate shortening, especially if the antiformal surface that is measured does not only result from buckling, but rather from an antiformal stack of several thrusts. Metamorphic *T* are compiled from literature data, which are derived from equilibrium parageneses, from RSCM analyses, and from closure *T* of thermochronological systems (Table S1 of supplementary material).

Shortening amounts shown in Fig. 7a are derived from measurements in the cover units for all external massifs and from line-length balancing in the Internal Massifs. This difference is due to the lack of appropriate markers other than the top of the basement surface in the Internal Massifs. On the other hand, most of the Internal Massifs (Gran Paradiso, Monte Rosa, Bergell) seem to consist of symmetric, ductile antiforms that did not form on top of coeval thrusts planes, suggesting that line-length balancing may be an appropriate technique to estimate shortening. Indeed, if the data are analysed separately for the External and for the Internal Massifs, positive correlations between metamorphic *T* and shortening are observed for both groups (Fig. 7).

Fig. 7b shows the massif height against the *T* of metamorphism. The massif height is simply defined as the distance between the hinge of the antiform taken at the top of the massif (from constructed sec-

tions) and the inferred basal detachment of the massif (see inset of Fig. 7b). For the Internal Massifs, where no basal detachment can be defined, it is taken as the distance between the hinge of the antiform at the basement-cover interface and the hinge of the synforms on both sides of the massif (it is twice the amplitude of the fold, as shown in the inset of Fig. 7b). Due to lateral gradients in the amplitude of the massifs, the height is measured where it is inferred to be the largest one in the massif. This representation (Fig. 7b) shows a good correlation between height and *T*, with no difference between internal and external massifs. The diagram shows a steepening of the best fit curve at the highest *T*, suggesting that increasing shortening does not lead anymore to increasing *T* in that range.

7. Discussion

7.1. Collisional shortening in the Alps

As shown in the compilations of Tables 1, 2, 3, the inferred amounts of shortening during Alpine collision vary significantly from one author to the other, especially in the Western Alps. We discuss below why the amounts of shortening estimated in the present study differ from those inferred in previous investigations.

7.1.1. Collisional shortening in the Western Alps

Different methods and different assumptions were used to quantify shortening in the Western Alps. *Lacassin (1989)*, based on a compilation of existing estimates, suggested that the "External structures", i.e. the European basement and cover, accommodated some 100 to 150 km of Cenozoic shortening. Many studies (Laubscher, 1991; Schmid and Kissling, 2000; Handy et al., 2010; Handy et al., 2015) used an "indirect" approach, by estimating the amount of deformation in the Central Alps, assuming a given amount of dextral strike-slip displacement along the Periadriatic Fault, and resolving these values by vector addition in a right angled triangle, whose hypotenuse provides both amount and direction of shortening in the Western Alps. Schmid and Kissling (2000) assumed 100 km of dextral strike-slip along the Periadriatic Fault, and a convergence direction oriented parallel to the Ecors traverse (N123°E; Fig. 1a), thus obtaining 124 km of post-Eocene shortening. Handy et al. (2010) resolved the estimated 63 km of N-S shortening of Schmid et al. (1996) for the post-32 Ma deformation north of the Periadriatic Fault on an inferred convergence direction of N123°E in the Western Alps, obtaining 243 km of shortening. The latter direction is the inferred average orientation of stretching lineations in the Western Alps, whose orientation however varies by ca. 120° along strike in the western Alpine arc. Finally, Handy et al. (2015) assumed 180 km for the post-35 Ma dextral offset along the Periadriatic Fault, thus obtaining 308 km of shortening for the post-35 Ma history along a N131°-oriented section in the Western Alps. Schmid et al. (2017) estimated shortening in the European crust of the Western Alps by area balancing on orogen-scale sections. This interpretation relies on several uncertainties, namely the correctly inferred geometry of the deep crust, and the existence of a decoupling horizon along the boundary between upper and lower crust, which would coincide with the geophysically defined boundary between the seismic velocities of 6.0 and 6.5 km/s (Schmid et al., 2017). They assessed some 27 km of shortening in the External Zone (along Ecors traverse; Fig. 1a), assuming a decoupling horizon at 17 km depth.

We emphasize, that in spite of the many difficulties associated with shortening estimates in the Western Alps, mainly due to the lack of appropriate markers in the Internal Zone, the approach used in this paper has the advantage of quantifying displacements directly from the observed structures, in cross sections and map view, across the entire western Alpine orogen.

Table 3
Compilation of literature data indicating inferred amounts of collisional shortening in the Eastern Alps.

Authors	Inferred amount and timing of N-S shortening	Area and method used for estimating shortening
Roeder, 1989	420 km post Late Oligocene shortening	Restoration of cross section across the entire orogen
Frisch et al., 1998 and 2000	113 km of post-Late Oligocene N-S shortening north of Periadriatic Fault. Shortening decreases to 40 km at the eastern margin of E-Alps.	Restoration of strike-slip displacements in map view, between Periadriatic Fault and northern front of Alps.
Schönborn, 1999	50 km of post-Eocene N-S shortening in the S-Alps	Restoration of balanced cross sections, between Periadriatic Fault and Southern front of the Alps (Bassano thrust)
Nussbaum, 2000	50 km of post-Oligocene N-S shortening in the S-Alps	Restoration of balanced cross sections between Periadriatic Fault and Southern front of the Alps, in the easternmost Southern Alps.
Linzer et al., 2002	61–64 km post-Oligocene shortening, north of Periadriatic Fault	Based on restoration of strike-slip displacements in map view between Periadriatic Fault and northernmost boundary of the N-Calcareous Alps
Rosenberg and Berger, 2009	149 km, post-Eocene shortening	Restoration of cross section, along TRANSALP, across the entire orogen
Favaro et al., 2017	75 km, post-30 Ma shortening north of Periadriatic Fault	Map view restoration, of strike-slip displacements between Periadriatic Fault and northernmost boundary of the N-Calcareous Alps
Rosenberg et al., 2018	65 km, post-Eocene shortening north of Periadriatic Fault	Map view restoration, of strike-slip displacements between Periadriatic Fault and northern tip of N-Calcareous Alps

7.1.2. Collisional shortening in the Central Alps

The inferred amounts of shortening in the Central Alps, as presented in Section 5, are larger than those suggested by previous literature (Table 2). Collisional shortening in the Central Alps was previously interpreted to have accommodated 125 km (Schmid et al., 1996; 1997; Schmid and Kissling, 2000; Handy et al., 2010), resulting from the sum of displacements in the south-verging thrusts of the Southern Alps (Schönborn, 1992), in the backthrust of the Periadriatic Fault, and in the north-verging thrusts of the Aar Massif. In addition, the offset between the front of the Austroalpine nappes and a marker arbitrarily chosen along the Moho was estimated by retro-deformation of the cross section and added to the latter values to obtain bulk shortening (Schmid et al., 1996; their Fig. 22-7f). Alternatively, Handy et al., (2015; their supplementary material) suggested that 160 km of N-S oriented shortening were accommodated across the NFP20 traverse (Figs. 1a and 2b) during collision. This value results from the sum of 95 km of inferred shortening in the Helvetic nappes (Pfiffner, 2009), 15 km in the Subalpine Molasse, and 50 km in the Southern Alps (Schönborn, 1992). Schmid et al. (2017) using the same procedure and assumptions described above for their assessment in the Western Alps, inferred 115 km of shortening in the European crust of the Central Alps, a value that is very close to that of Handy et al. (2015).

Our estimates presented in Section 5 and Fig. 5 is based, as the studies above, on shortening amounts constrained by Schönborn (1992) for the Southern Alps, but displacements north of the Periadriatic Fault are newly calculated, and they provide higher values than in previous studies (144 km along the NFP20 section, without including dextral strike slip along the Periadriatic Fault; Fig. 5). This difference results from the fact that we consider shortening accommodated in the coupled Subalpine Molasse/Aar Massif system to have attained 50 km (Ortner et al., 2015), that we include in our calculation shortening accommodated by the Glarus thrust (35 km), and that we also take into account the *syn*-collisional part of displacement of the Penninic Front (35 km; Fig. 5).

Finally, we also include 100 km dextral strike-slip displacement of the Periadriatic Fault, thus obtaining 223 km of bulk shortening across the orogen, along a northwest-oriented direction in the part of the Central Alps.

Our estimates above suggest that shortening in the Central Alps is significantly larger than in the Western Alps (Fig. 5). Qualitatively, this difference is well illustrated by the different geometry of the Penninic Front. Its surface expression in the Western Alps can be followed into a series of planar seismic reflectors dipping approximately at 40° to the east in the middle crust (> 15 km depth; e.g., Tardy et al., 1990). These reflectors are inferred to flatten eastward before they re-steepen and attain a depth of 60 km along the interface between the European and the Adriatic Mohos (Schmid and Kissling, 2000; Cross Section 1 in Fig. 8). As shown by the cross sections of Fig. 8, the Penninic Front represents the surface expression of an >100 km long thrust, whose geometry passes from a planar surface in the south (Section 1 in Fig. 8) to an increasingly folded surface further north and northeastward. In the northern part of the Western Alps (Section 3 in Fig. 8), this large-scale thrust is folded by two antiforms: one above the Aar Massif and one below the internal Monte Rosa Massif (e.g., Schmid and Kissling, 2000). In the internal Central and Eastern Alps, the Penninic Front is folded by larger amplitude folds (Sections 4 and 5 in Fig. 8), indicating significant shortening after its activity.

7.1.3. Collisional shortening in the Eastern Alps

Recently estimated amounts of shortening in the Eastern Alps (Favaro et al., 2017; Rosenberg et al., 2018) are smaller compared to previous literature (e.g., Frisch et al., 1998, 2000; Linzer et al., 2002; Ustaszewski et al., 2008). This difference results from different amounts of inferred orogen-parallel extension. Whereas Frisch et al. (1998, 2000) and Ustaszewski et al. (2008) estimated 180 km of *E*-W orogen-parallel extension, Rosenberg et al. (2015, 2018) and Favaro et al. (2017) concluded on the base of map-view retro-deformation of strike-slip displacements that E-W extension only attained some 75 km. Lower amounts of orogen-parallel extension inevitably lead to smaller amounts of orogen perpendicular shortening in map-view restorations (Favaro et al., 2017; Rosenberg et al., 2018).

Summing up shortening in the Eastern Alps, south and north of the Periadriatic Fault, results in 160 km along sections striking through the western Tauern Window (Fig. 5) and 145 km along sections crossing the eastern Tauern Window (Fig. 5). Hence, a significant decrease in the amount of shortening appears to take place from west to east when passing from the Central to the Eastern Alps. This decrease is mainly governed by differences of shortening in the Southern Alps (Fig. 5).

An eastward decrease of shortening is not consistent with collision governed by the anticlockwise rotation of Adria around a pole located in the western Alps, close to Torino (Fig. 1a), as suggested by GPS-based velocity models (Westaway, 1990; Ward, 1994; Calais et al., 2002). This eastward decrease in the amount of collisional shortening suggests that the amount of anticlockwise rotation of Adria must have been modest during collision. This conclusion is consistent with recent paleogeographic reconstructions of the peri-Alpine realm, suggesting a rotation of 5° since 20 Ma (Le Breton et al., 2017).

7.2. Convergence amount and direction of Adria-Europe during collision

Recent paleogeographic reconstructions of the Tertiary Alpine realm suggested a WNW motion of Adria since the Upper Oligocene (Handy et al., 2010; Handy et al., 2015; Schmid et al., 2017). However, the amount of collisional shortening in the Western Alps, as estimated

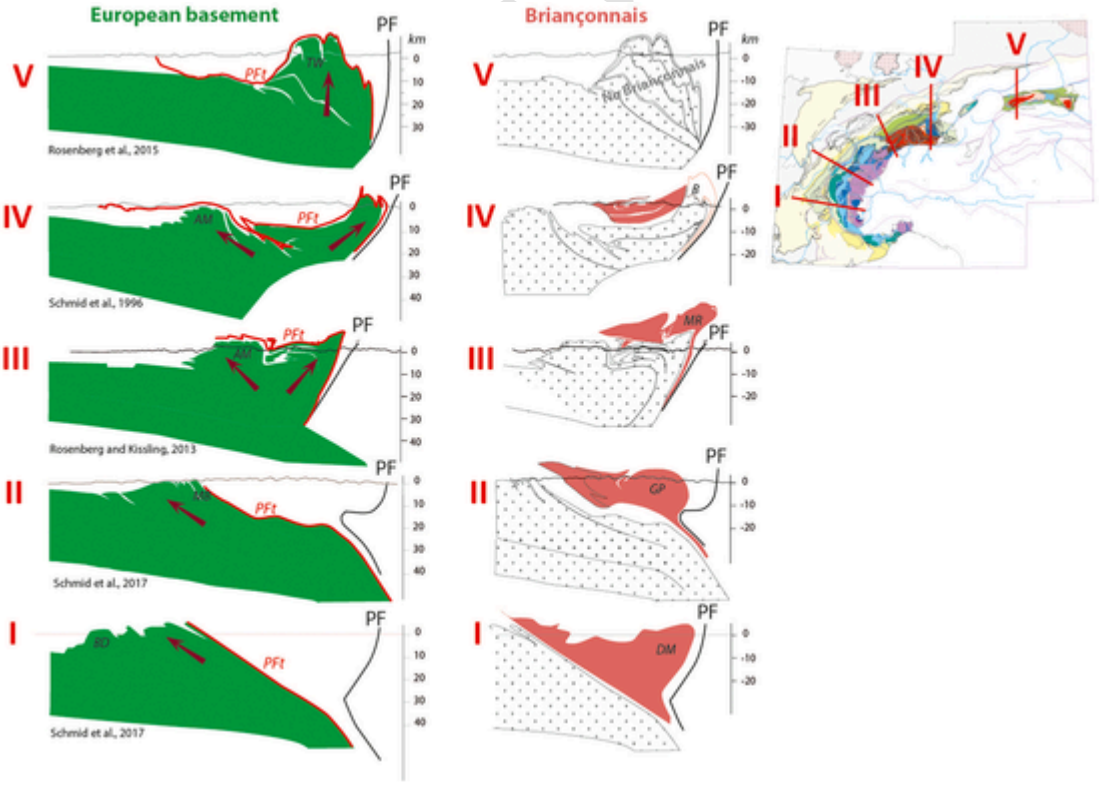

Fig. 8. Sections highlighting cross-sectional surface and geometry of the Briançonnais-derived and the Europe-derived parts of the orogenic wedge. Red arrows indicate the displacement direction of the orogenic wedge as a consequence of collisional shortening. Where a thick part of the orogenic wedge consists of Briançonnais units, collisional shortening and exhumation are displaced towards the foreland. Progressively thinner Briançonnais units are correlated with larger amounts of shortening and exhumation in the interal part of the orogenic wedge. Inset map shows section traces. *PFt*: Penninic Front; PF: Periadriatic Fault. AM: Aar Massif; B: Bergell Pluton; BD: Belledonne Massif; DM: Dora Maira Massif; GP: Gran Paradiso Massif; MB: Mont Blanc Massif: MR: Monte Rosa Massif; TW: Tauern Window. (For interpretation of the references to colour in this figure legend, the reader is referred to the web version of this article.)

in this study, is smaller by a factor of approximately 2 with respect to previous studies (Table 1), and the amount of shortening inferred for the Central Alps in this study is larger than previously suggested (Table 2). Therefore, if the convergence direction of Adria during collision can be reconstructed based on map-view distribution of shortening (Fig. 5), it must have been approximately 330°. This orientation is almost exactly parallel to the one independently inferred from recent paleogeographic reconstructions (338°, van Hinsbergen et al., 2020; 335°, Le Breton et al., 2021), which are mainly based on large scale fit of conjugate magnetic anomalies of the Atlantic. These studies suggest that Alpine convergence during collision corresponded to 210 km (van Hinsbergen et al., 2020), or 260 km (Le Breton et al., 2021). Our estimate (Fig. 5) along the NNW-oriented transect indicates more than 200 km of shortening, thus a value that is consistent with the ones above inferred for convergence during collision. In addition, a NNW-oriented convergence direction is also inferred from paleomagnetic reconstructions of Adria throughout the Miocene (e.g., Dewey et al., 1989; Faccenna et al., 2004).

7.3. Map view distribution of Barrovian metamorphism and collisional shortening

As mentioned above, post-30 Ma Barrow-type metamorphism is discontinuously exposed along strike in the Alps. In addition, its occurrence in map view in the Western Alps is limited to the External Zone, where its highest *T* values are significantly lower than those recorded in the Lepontine and Tauern domes. Greenschist facies metamorphism was recognized to overprint HP metamorphism in the Internal Zone of the Western Alps, but it is poorly dated, mostly Late Eocene, and only locally continuing into the Early Oligocene (Gerber, 2008) collisional stage. These observations raise the following questions: (1) why, from 30 Ma onward, is the Internal Zone not affected by Barrovian metamorphism, in contrast to the External Zone of the Western Alps, and (2) why is the temperature of collisional metamorphism in the Western Alps lower than in the Central Alps?

(1) Concerning the first question, it can be stated that collisional shortening was modest in the Internal Zone of the Western Alps, as discussed above (Sections 5.1 and 7.1.1) and shown in Fig. 5, hence exhumation was modest too. Although some collision-related deformations are documented in the Briançonnais and Schistes Lustrés domains (Bucher et al., 2003; Tricart and Schwartz, 2006), these deformations remain to be dated and quantified in terms of their amount of shortening. As shown for the Gran Paradiso Massif (Section 2 in Fig. 8), collisional shortening was insufficient to exhume rock units whose zircon fission track ages are reset to the time of collision. The very significant amounts of deformation and exhumation in this area are almost entirely confined to its subduction stage, as shown by cooling ages (Malusà et al., 2005) and by detritic thermochronological data from the Tertiary Piemont Basin (southwestern Po Plain). These data show that $^{40}Ar/^{39}Ar$ ages of detrital minerals derived from *HP* rocks of the Internal Zone (Carrapa et al., 2003) remain very similar (around 38 Ma) throughout 9 different stratigraphic units corresponding to the depositional time range between 30 Ma and the present (Carrapa et al., 2003). As a consequence, no significant exhumation nor vertical movements took place in the Internal Zone of the Western Alps after 30 Ma, otherwise detrital minerals with progressively younger cooling ages would be found in younger stratigraphic units, as observed in the Molasse Basin of the Central Alps (von Eynatten et al., 1999). These relationships are different in the External Zone of the Western Alps, where shortening is more significant (Sections 5.1 and 7.1.1), hence zircon fission tracks are partly reset to Miocene ages, and metamorphic *T* reach at least 400 °C (Fig. 1b).

(2) Concerning the differences of *syn*-collisional metamorphic *T* between Western and Central Alps, and considering the above described correlation between amount of shortening and *T* of metamorphism (Fig. 7), the smaller amounts of collisional shortening inferred for the Western Alps in this study provide a simple answer. Smaller amounts of shortening lead to smaller amounts of thickening and erosion, hence lesser exhumation and lower metamorphic *T* in rocks presently exposed at the surface. In addition, the accommodation site of these smaller amounts of shortening in the Western Alps shifted to the External Zone, thus exposing Barrow metamorphic belt in a more external position compared to the Central Alps (Fig. 3). This shift in the deformation pattern is responsible for the formation of the External Massifs and the Chaînes Subalpines in the Western Alps.

The observations above raise an additional question concerning the causes of localization of shortening in the External Zone in the Western Alps vs localization both in the External and Internal Zone in the Central and Eastern Alps. At the onset of collision, the structure of the Western and Central Alps differs in at least one major point that may control the future site of shortening during collision: the thickness of the Briançonnais nappes. As shown in Fig. 8, the Briançonnais nappe stack progressively decreases its thickness from south to north in the Western Alps, becoming even thinner in the Central Alps, and completely disappearing at the eastern termination of the Central Alps. Progressive thinning of the Briançonnais nappe pile goes together with increased shortening and thickening of the European basement (Fig. 8, Sections 3 to 4). Where the Briançonnais nappe stack is completely absent, as in the Eastern Alps, shortening is almost entirely localized in the internal part of the chain, where the amplitude of the antiformal stack of Europe-derived basement nappes is largest (Fig. 8, Section 5). The presence of an intermediate continental slice (Briançonnais) that was subducted and exhumed before the larger (European) continental margin entered the subduction zone, modified the style of collisional deformation. While this exhumed slice becomes accreted to the upper plate, the active site of shortening shifts towards the foreland. Hence, deformation of the European margin takes place in a more external position, because the upper plate itself grows towards the foreland by accretion of the exhumed Briançonnais nappes.

As shown in Fig. 7a, shortening percentages of individual basement massifs show a positive correlation with the *T* attained by these massifs during Alpine collision, but an even better correlation is obtained if the height of the massifs is plotted against the *T* (Fig. 7b). A major reason for the different *T* vs shortening correlations between Internal and External Massifs (Fig. 7a) probably lies in the difficulty of calculating shortening in the Internal Massifs, where it is generally performed by line-length balancing of their reconstructed basement-cover surface, possibly underestimating bulk shortening. In contrast, shortening in the External Massifs can be calculated indirectly, by extrapolating displacements of cover thrusts that are known to root in the basement, or by assuming a specific mode of shortening in the basement. Different modes of shortening may correspond to the same amplitude and thickening of the basement massif (e.g., Burkhard, 1990; Herwegh et al., 2020), but to different amounts of bulk shortening.

The height of the massifs, as defined in Fig. 7b, represents the amount of tectonic uplift of the uppermost massif surface due to shortening. The height of the antiformal stacks forming the massifs is more directly related to the paths of material particles towards the surface (Fig. 9). Hence, the positive correlation between shortening and metamorphic *T* (Fig. 7b) is due to the link between the amount of uplift and exhumation and the amount of shortening.

Paleogeographic solutions relate the changes in the degree of syn-collisional metamorphism to changes in the geometry of the paleo-European margin (Goffé et al., 2003). Different parts of the margin enter the subduction zone at different times, thereby causing lateral

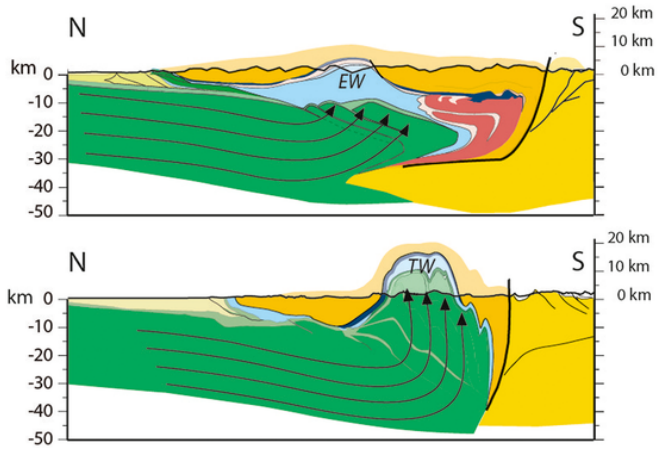

Fig. 9. Engadine (EW) vs Tauern (TW) Windows. Black lines and associated arrows indicate inferred, simplified particle paths during burial and exhumation. Shortening and exhumation are larger in the Tauern Window and they are localized in a more internal part of the orogen. The latter brings particle paths to a deeper structural level. Larger amounts of shortening induces larger uplift and exhumation of these particles. Legend as in Fig. 2.

changes in the thickness of the continental nappe pile. Where continental subduction initiates first, it creates a stack of highly radiogenic (> 2.5 μWm^{-3}; e.g., Vilà et al., 2010) basement nappes, capable of generating *HT* metamorphism (Goffé et al., 2003). Alternatively, based on the correlations between amounts of shortening, the height (uplift) of the metamorphic massif antiforms and the *T* of metamorphism (Fig. 7), it may be concluded that the maximum *T* attained during collision by metamorphic rocks now exposed at the surface depends on the amplitude of antiformal folding of a given massif, which is related to the amount of collisional shortening. This conclusion, which is supported by the data of Fig. 7, neglects the contribution of processes such as radioactive decay and advective heat transport (Berger et al., 2011) during and after thickening. These processes certainly affected the maximum metamorphic *T* during collision, and their effect may explain the steepening of the best fit curve at the highest *T* (Fig. 7b), suggesting no direct control of shortening on metamorphic *T* in this higher *T* range. Indeed the maximum *T* of collisional metamorphism locally persisted until 20 Ma in the southern Lepontine dome (Rubatto et al., 2009), hence at a time when collisional shortening and exhumation were already well developed in the Central Alps.

A comparison of metamorphism in the Engadine and the Tauern Window shows that the Valais nappes in these areas, in spite of their common paleogeographic origin and their similar structural position within the orogenic wedge, are affected by different metamorphic temperatures during collision. Whereas the present exposure of Valais-derived nappes in the Engadine Window does not exceed 300 °C, the same units attained 600 °C in the Tauern Window (Hoernes and Friedrichsen, 1974; Rosenberg et al., 2018). As shown in Fig. 9, these units are in the same structural position in both windows, namely immediately above the European basement and its cover nappes. The lack of a 2 km thick Briançonnais nappe in the hangingwall of these Valais Units within the Tauern Window is unlikely to have induced significant differences in the *T* of collisional metamorphism, and if it did so, it would increase the *T* of the Valais nappes in the Engadine Window, hence not explaining their lower *T*. From a structural point of view, two first-order differences exist among these areas (Fig. 9): first, the Valais nappes exposed in the Engadine Window are >10 km above the top of the European basement, whereas they are verticalized and exposed at the surface at the same level of the European basement in the Tauern Window, due to larger amounts of shortening and exhumation (Fig. 9). Second, shortening and exhumation localized in a more internal part of the orogen in the Tauern Window. Material points exposed at the surface in such areas follow particle paths that reached significantly deeper crustal levels(Fig. 9), before being exhumed to the surface, assuming material particles follow displacement paths as suggested by shortening experiments coupled with erosion (e.g., Batt and Braun, 1997; Willett et al., 1993; Willett and Brandon, 2002; Simoes et al., 2007). Therefore, rocks derived from the same tectonic unit (e.g., Valais nappes) in the Engadine and Tauern Windows show different metamorphic conditions, because they followed different burial and exhumation paths (Fig. 9).

The above described models assume that exhumation of the metamorphic windows takes place by erosion associated to large-scale folding and thickening. In case of the Tauern Window crustal volumes with a vertical extent of up to 25–30 km (assuming 10–15 km thickness for the eroded Austroalpine nappes) must have been eroded. This value is consistent with the inferred *P* of 0.7 to 0.9 GPa inferred for the latter area between 30 and 34 Ma (Selverstone, 1993). A comparison between rates of exhumation calculated from cooling ages of thermochronometers and from the inferred eroded nappe pile shown in cross sections and averaged over 30 Ma (collisional phase), shows a rather good agreement between the two independent estimates (Rosenberg et al., 2015). Therefore, exhumation mainly driven by erosion is likely. Erosion rates attain 1.2 mm/a in the most exhumed (during collision) parts of the orogen, whereas they only reach 0.1 mm/a in the less exhumed parts (Rosenberg et al., 2015; their Fig. 6).

In summary, the comparison between Tauern Window and Engadine Window shows that the difference of metamorphism attained in the same unit is likely due to very different amounts of shortening associated with larger burial and exhumation in case of the Tauern Window. Therefore, no paleogeographical arguments (Goffé et al., 2003) are needed to explain these differences in P-T conditions.

7.4. Conceptual model explaining along-strike differences in the distribution of shortening and metamorphism

The discussion above is summarized and simplified in the three sketches of Fig. 10, which schematically relate the first-order differences in the spatial distribution of collisional shortening and exhumation (hence metamorphism exposed at the surface) to the presence or absence of an exhumed Briançonnais nappe pile at the onset of collision. Where a thick stack of Briançonnais nappes is exhumed and accreted to the upper plate before the onset of collision, as in the Western Alps (Fig. 10), the site of collisional shortening shifts towards the foreland, where it forms the belt of External Massifs. In contrast, where the Briançonnais nappe pile is absent, as in the Eastern Alps (Fig. 10), the site of major collisional shortening remains in the Internal Zone of the chain, adjacent to the South Alpine indenter, throughout the collisional history. Where the Briançonnais nappes are present but without a significant thickness, as in the Central Alps (Fig. 10), an intermediate situation develops, in which collisional shortening is more distributed across the Alpine belt, forming an-orogen scale antiform in the Internal Zone and a second one in the External Zone.

The degree of collisional metamorphism recorded in the exhumed units is proportional to the amount of exhumation, which is itself related to the amount of shortening. The higher *T* attained in the Central Alpine and the Eastern Alpine domes (Lepontine and Tauern, Fig. 1), compared to the western Alpine External Massifs is due to lower amounts of collisional shortening accommodated in the latter area.

8. Conclusions

In spite of methodological limitations on quantifying absolute amounts of shortening, especially within the internal basement units, our reassessment of displacements accommodated by the major collisional structures shows that collisional shortening in the Central Alps is likely to be larger than previously estimated and it is larger than in the

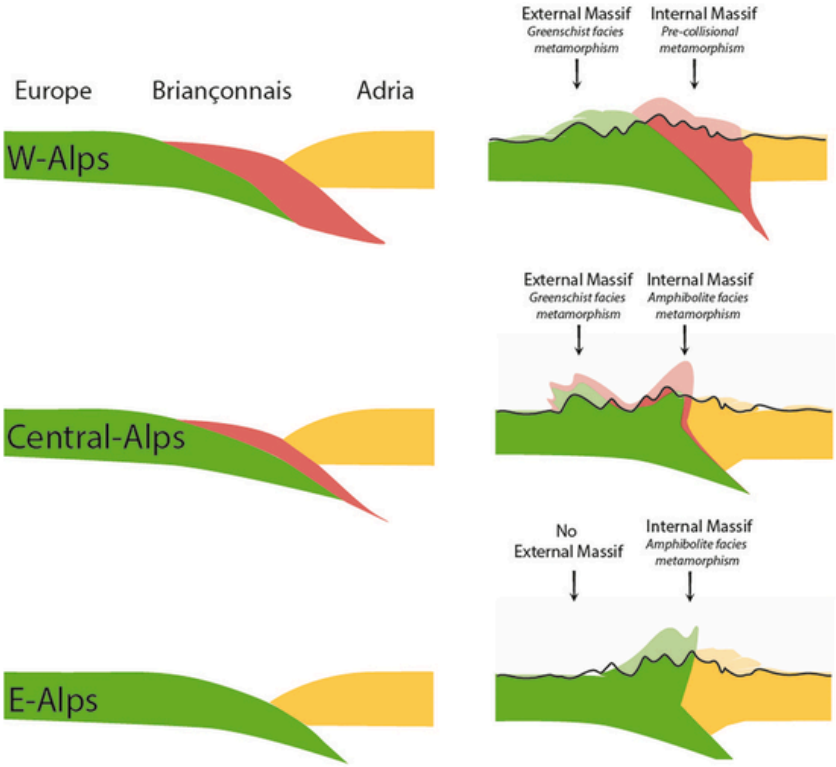

Fig. 10. Conceptual model, showing how style of shortening and degree of collisional metamorphism vary along strike in the Alps as a function of bulk collisional shortening and size of Briançonnais domain. Western Alps: bulk collisional shortening is modest, Briançonnais Domain is large and collisional shortening mainly localizes in the External Zone. Syn-collisional metamorphism only attains greenschist facies and it is only exposed in the External Zone. Central Alps: Bulk collisional shortening is highest, Briançonnais Domain is thin and involved in shortening structures with the European basement. Shortening localizes both in the Internal and External Zone of the orogen. Collisional metamorphism attains amphibolite facies in the Internal Zone and greenschist facies in the External Zone. Eastern Alps: Briançonnais Domain is absent, thus collisional shortening localizes in the internal part of the orogen, where amphibolite facies metamorphism develops.

Western and in the Eastern Alps. Shortening values calculated in this manuscript are inferred by analyzing a small number of large, first-order structures of the Alpine collisional wedge. More homogeneous shortening by layer-parallel thickening and deformation on smaller-scale structures is not taken into account. Therefore, the absolute values presented above must be considered as minimum values.

In addition to the Lepontine and Tauern domes, Barrovian metamorphism affects the western and northwestern Alps all along an orogen-parallel belt in the external part of the Alpine Chain, which accommodates the largest amount of collisional shortening in the Western Alps. Both the peak *T* and the amount of shortening attained along this belt, are systematically lower than those attained in the Lepontine and Tauern domes.

As a consequence of the distribution of shortening in map view, indicating that its amount gradually decreases from the Central to the Western Alps, where the strike direction of the Chain becomes closer to N-S, we suggest that convergence during collision was oriented NNW rather than WNW, as commonly concluded in previous literature.

Shortening percentages in the basement massifs correlate with the metamorphic *T* that they attained during collision. However a better correlation is shown between massif height (vertical extension) and *T*, suggesting that the amount of vertical thickening and uplift are the main factors controlling the metamorphic *T* during collision.

The position of the areas affected by Barrovian metamorphism depends on the localization of collisional shortening, which takes place in the external part of the Chain in the Western Alps, but largely in a more internal part in the Central and Eastern Alps. This difference in the area of localization appears to be controlled by the presence of the Briançonnais nappe stack. These nappes, subducted and exhumed prior to collision, form a large wedge in the Western Alps, but only a very thin one in the Central Alps, and they completely disappear in the Eastern Alps. Where they form a larger wedge, they become part of the "back stop" and collisional shortening shifts towards the foreland, forming the External Massifs. Where the Briançonnais wedge is absent, as in the Eastern Alps, shortening localizes almost entirely in the Internal Zone. Where it is very thin, as in the Central Alps, collisional shortening is distributed both in the internal and external domains.

Supplementary data to this article can be found online at https://doi.org/10.1016/j.earscirev.2021.103774.

Uncited references

Berger and Bousquet, 2008
Bousquet et al., 2008
Butler, 1983
Butler et al., 1986
Cederboom et al., 2011
Cenki-Tok et al., 2013
Challandes et al., 2008
Fumasoli, 1975
Herwegh et al., 2017
Kirschner et al., 1996
Kissling, 2008
Lippitsch et al., 2003
Mancktelow and Pavlis, 1994
Métois et al., 2015
Mitterbauer et al., 2011
Platt, 1984
Rolland, 2014
Schmid and Froitzheim, 1993

Schmid et al., 2004

Declaration of Competing Interest

The authors declare that they have no known competing financial interests or personal relationships that could have appeared to influence the work reported in this paper.

Acknowledgements

Hugo Ortner, Jean Baptiste Girault, and Romain Bousquet are kindly acknowledged for constructive discussions on several aspects of this paper. JB Girault generously provided a compilation of RSCM data of the Western Alps. Romain Bousquet stressed already long time ago that collisional shortening in the Western Alps is not as large as in the other parts of the Chain. An anonymous reviewer, Kurt Stüwe and Stefan Schmalhoz reviewed this manuscript. Kurt Stüwe and Stefan Schmalholz provided very constructive reviews, which improved the quality of the manuscript and figures. Gerit Gradwohl performed a very rigorous and helpful screening of our text.

References

Argand, E., 1916. Sur l'arc des Alpes Occidentales. Eclogae Geol. Helv. 14, 145–191.
Bartosch, T., Stüwe, K., Robl, J., 2017. Topographic evolution of the Eastern Alps: the influence of strike-slip faulting activity. Lithosphere 9, 384–398.
Batt, G.E., Braun, J., 1997. On the thermo-mechanical evolution of compressional orogens. Geophys. J. Int. 128, 364–382.
Bellahsen, N., Mouthereau, F., Boutoux, A., Bellanger, M., Lacombe, O., Jolivet, L., Rolland, Y., 2014. Collision kinematics in the western external Alps : Kinematics of the Alpine collision. Tectonics 33, 1055–1088.
Bellanger, Y.M., Augier, R., Bellahsen, N., Jolivet, L., Monié, P., Baudin, T., Beyssac, O., 2015. Shortening of the European Dauphinois margin (Oisans Massif, Western Alps): new insights from RSCM maximum temperature estimates and 40Ar/39Ar in situ dating. J. Geodyn. 83, 37–64.
Berger, A., Bousquet, R., 2008. Subduction-related metamorphism in the Alps: Review of isotopic ages based on petrology and their geodynamic consequences. In: Siegesmund, S., Fügenschuh, B., Froitzheim, N. (Eds.), Tectonic Aspects of the Alpine-Dinaride-Carpathian System, Vol. 298. Geol. Soc. Spec. Publ, London, pp. 117–144.
Berger, A., Schmid, S.M., Engi, M., Bousquet, R., Wiederkehr, M., 2011. Mechanisms of mass and heat transport during Barrovian metamorphism: a discussion based on field evidence from the Central Alps (Switzerland/northern Italy). Tectonics 30, TC1007.
Berger, A., Engi, M., Erne-Schmid, S., Glotzbach, C., Spiegel, C., de Goede, R., Herwegh, M., 2020. The relation between peak metamorphic temperatures and subsequent cooling during continent-continent collision (western Central Alps, Switzerland). Swiss J. Geosci. 113, 1–18.
Bertrand, A., Rosenberg, C.L., Garcia, S., 2015. Fault slip analysis and late exhumation of the Tauern Window, Eastern Alps. Tectonophysics 649, 1–17.
Bigioggero, B., Tunesi, A., 1988. The "Valle del Cervo" plutonic body. Notes to the field trip on 1st October, 1987. Rend. Soc. Ital. Mineral. Petrol. 43, 355–366.
Bigot-Cormier, F., Poupeau, G., Sosson, M., 2000. Dénudations différentielles du massif cristallin externe alpin de l'Argentera (Sud-Est de la France) révélées par thermochronologie traces de fission (apatites, zircons). C. R. Acad. Sci. Ser. IIA Earth Planet. Sci. 330, 363–370.
Borsi, S., Del Moro, A., Sassi, F., 1973. Metamorphic evolution of the Austridic rocks to the south of the Tauern Window (Eastern Alps): radiometric and geopetrological data. Mem. Soc. Geol. Ital. 12, 549–571.
Bousquet, R., Oberhänsli, R., Goffé, B., Wiederkehr, M., Koller, F., Schmid, S.M., Schuster, R., Engi, M., Berger, A., Martinotti, G., 2008. Metamorphism of metasediments at the scale of an orogen: A key to the Tertiary geodynamic evolution of the Alps. In: Siegesmund, S., Fügenschuh, B., Froitzheim, N. (Eds.), Tectonic Aspects of the Alpine-Dinaride-Carpathian System, Vol. 298. Geol. Soc. Spec. Publ, London, pp. 393–411.
Bousquet, R., Oberhänsli, R., Schmid, S.M., Berger, A., Wiederkehr, M., Robert, C., Rosenberg, C.L., Koller, F., Molli, G., Zeilinger, G., 2012a. Tectonic Framework of the Alps CCGM/CGMW.
Bousquet, R., Oberhänsli, R., Schmid, S.M., Berger, A., Wiederkehr, M., Robert, C., Rosenberg, C.L., Koller, F., Molli, G., Zeilinger, G., 2012b. Metamorphic Framework of the Alps CCGM/CGMW.
Boutoux, A., Bellahsen, N., Nanni, U., Pik, R., Verlaguet, A., Rolland, Y., Lacombe, O., 2016. Thermal and structural evolution of the external Western Alps: Insights from (U–Th–Sm)/he thermochronology and RSCM thermometry in the Aiguilles Rouges/Mont Blanc massifs. Tectonophysics 683, 109–123.
Bucher, S., Schmid, S.M., Bousquet, R., Fügenschuh, B., 2003. Late-stage deformation in a collisional orogen (Western Alps): nappe refolding, back-thrusting or normal faulting?. Terra Nova 15, 109–117.
Bucher, S., Ulardic, C., Bousquet, R., Ceriani, S., Fügenschuh, B., Gouffon, Y., Schmid, S. M., 2004. Tectonic evolution of the Briançonnais units along a transect (ECORS-CROP) through the Italian-French Western Alps. Eclogae Geol. Helv. 97, 321–345.
Burg, J.-P., Gerya, T.V., 2005. The role of viscous heating in Barrovian metamorphism of collisional orogens: thermomechanical models and application to the Lepontine Dome in the Central Alps. J. Metamorph. Geol. 2005 (23), 75–95.
Burkhard, M., 1988. L'Helvétique de la bordure occidentale du massif de l'Aar (évolution tectonique et métamorphique). Eclogae Geol. Helv. 8, 63–114.
Burkhard, M., 1990. Aspects of the large-scale Miocene deformation in the most external part of the Swiss Alps (Subalpine Molasse to Jura fold belt). Eclogae Geol. Helv. 83, 559–583.
Burkhard, M., Sommaruga, A., 1998. Evolution of the western Swiss Molasse basin: Structural relations with the Alps and the Jura belt. Geol. Soc. London Spec. Publ. 134, 279–298. https://doi.org/10.1144/GSL.SP.1998.134.01.13.
Butler, R.W.H., 1983. Balanced cross-sections and their implications for the deep structure of the Northwest Alps. J. Struct. Geol. 5, 125–137.
Butler, R.W.H., 1985. The restoration of thrust systems and displacement continuity around the Mont Blanc massif, NW external Alpine trust belt. J. Struct. Geol. 7, 569–582.
Butler, R.W.H., Matthews, S.J., Parish, N., 1986. The NW external Alpine Thrust Belt and its implications for the geometry of the Western Alpine Orogen. Geol. Soc. Lond. Spec. Publ. 19, 245–260.
Calais, E., Noquet, J.-M., Jouanne, F., Tardy, M., 2002. Current Extension in the Central part of the Western Alps from continuous GPS measurements, 1996–2001. Geology 30–7, 651–654.
Campani, M., Herman, F., Mancktelow, N.S., 2010. Two- and three-dimensional thermal modeling of a low-angle detachment: Exhumation history of the Simplon Fault Zone, Central Alps. J. Geophys. Res. 115, B10420. https://doi.org/10.1029/2009JB007036.
Cardello, G.L., Di Vincenzo, G., Giorgetti, G., Zwingmann, H., Mancktelow, N.S., 2019. Initiation and development of the Pennine Basal Thrust (Swiss Alps): a structural and geochronological study of an exhumed megathrust. J. Struct. Geol. 126, 338–356.
Carrapa, B., Wijbrans, J., Bertotti, G., 2003. Episodic exhumation in the Western Alps. Geology 31, 601–604.
Cederboom, C.E., van der Beek, P., Schlunegger, F., Sinclair, H.D., Oncken, O., 2011. Rapid extensive erosion of the North Alpine foreland basin at 5–4 Ma. Basin Res. 23, 528–550. https://doi.org/10.1111/j.1365-2117.2011.00501.x.
Cenki-Tok, B., Darling, J.R., Rolland, Y., Dhuime, B., Storey, C.D., 2013. Direct dating of mid-crustal shear zones with synkinematic allanite: New in situ U–Th–Pb geochronological approaches applied to the Mont Blanc massif. Terra Nova 26, 29–37. https://doi.org/10.1111/ter.12066.
Ceriani, S., Fügenschuh, B., Schmid, S.M., 2001. Multi-stage thrusting at the "Penninic Front" in the Western Alps between Mont Blanc and Pelvoux massifs. Int. J. Earth Sci., (Geol. Rundsch.) 90, 685–702.
Challandes, N., Marquer, D., Villa, I.M., 2008. PTt modelling, fluid circulation, and ^{39}Ar-^{40}Ar and Rb-Sr mica ages in the Aar Massif shear zones (Swiss Alps). Swiss J. Geosci.. https://doi.org/10.1007/s00015-008-1260-6.
Cliff, R.A., Oberli, F., Meier, M., Droop, G.T.R., Kelly, M., 2015. Syn-metamorphic folding in the Tauern Window, Austria dated by Th–Pb ages from individual allanite porphyroblasts. J. Metamorph. Geol. 33, 427–435.
Corsini, M., Ruffet, G., Caby, R., 2004. Alpine and late hercynian geochronologicalconstraints in the Argentera Massif (Western Alps). Eclogae Geol. Helv. 97, 3–15.
Crouzet, C., Ménard, G., Rochette, P., 1999. High-precision three-dimensional paleothermometry derived from paleomagnetic data in an Alpine metamorphic unit. Geology 27, 503–506.
Debelmas, J., Kerckhove, C., 1980. Les Alpes franco-italiennes. Géol. Alpine 56, 21–58.
Dewey, J.F., Helman, M.L., Turco, E., Hutton, D.H.W., Knot, S.D., 1989. Kinematics of the western Mediterranean. In: Coward, M.P., Dietrich, D., Park, R.G. (Eds.), 1989, Alpine Tectonics, Geological Society Special Publication No. 45. pp. 265–283.
Doglioni, C., 1992. The venetian Alps thrust belt. In: McKlay, K. (Ed.), Thrust Tectonics. Springer, Dordrecht, pp. 319–324.
Engi, M., Berger, A., Roselle, G.T., 2001. Role of the accretion channel in collisional orogeny. Geology 29, 1143–1146.
Engi, M., Bousquet, R., Berger, A., 2004. Explanatory notes to the map: Metamorphic structure of the Alps, Central Alps. Mitt. Österr. Mineral. Ges. 149, 157–173.
England, P.C., 1978. Some thermal considerations of the Alpine metamorphism – past, present and future. Tectonophysics 46, 21–40.
England, P.C., Richardson, S.W., 1979. The influence of erosion upon the mineral facies of rocks from different metamorphic environments. J. Geol. Soc. Lond. 134, 201–213.
Ernst, W.G., 1971. Metamorphic zonations on presumably subducted lithospheric plates from Japan, California and the Alps. Contrib. Mineral. Petrol. 34, 43–59.
Ernst, W.G., 1973. Interpretive synthesis of metamorphism in the Alps. Geol. Soc. Am. Bull. 84, 2053–2078.
Evans, S.L., 2011. Timing of Exhumation of the Eastern Central Alps from Zircon and Apatite (U-Th)/He Thermochronology (Graubunden, Switzerland). University of Kansas, MSc. Thesis, p. 226.
Faccenna, C., Piromallo, C., Crespo-Blanc, A., Jolivet, L., Rossetti, F., 2004. Lateral slab deformation and the origin of the western Mediterranean arcs. Tectonics 23, TC1012. https://doi.org/10.1029/2002TC001488.
Favaro, S., Handy, S.M., Scharf, A., Schuster, R., 2017. Changing patterns of exhumation and denudation in front of an advancing crustal indenter, Tauern Window (Eastern Alps). Tectonics 36, 1053–1071. https://doi.org/10.1002/2016TC004448.
Fox, M., Herman, F., Willett, S.D., Schmid, S.M., 2016. The exhumation history of the European Alps inferred from linear inversion of thermochronometric data. Am. J. Sci. 316 (June, 2016), 505–541. https://doi.org/10.2475/06.2016.01.
Frey, M., Hunziker, J.C., Frank, W., Bocquet, J., Dal Piaz, G.V., Jäger, E., Niggli, E., 1974. Alpine metamorphism of the Alps: a review. Schweiz. Mineral. Petrogr. Mitt. 54, 247–290.
Frisch, W., Kuhlemann, A., Dunkl, I., Brügel, A., 1998. Palinspastic reconstruction and topographic evolution of the Eastern Alps during late Tertiary tectonic extrusion. Tectonophysics 297, 1–15.

Frisch, W., Dunkl, I., Kuhlemann, J., 2000. Postcollisional orogen-parallel large-scale extension in the Eastern Alps. Tectonophysics 327, 239–265.
Froitzheim, N., Schmid, S.M., Frey, M., 1996. Mesozoic paleogeography and the timing of eclogite facies metamorphism in the Alps: a working hypothesis, Eclogae Geol. Helv. 89, 81–110.
Fügenschuh, B., Schmid, S.M., 2003. Late stages of deformation and exhumation of an orogen constrained by fission-track data: a case study in the Western Alps. Geol. Soc. Am. Bull. 115, 1425–1440.
Fumasoli, M., 1975. Geologie des Gebietes nördlich und südlich der Jorio-Tonale-Linie im Westen von Gravedona. Mitt. Geol. Inst. Eidg. Tech. Hochsch. Univ. Zürich 194, 1–230.
Gabalda, S., Beyssac, O., Jolivet, L., Agard, P., Chopin, C., 2009. Thermal structure of a fossil subduction wedge in the Western Alps. Terra Nova 28–34.
Garzanti, E., Malusà, M., 2008. The Oligocene Alps: Domal unroofing and drainage development during early orogenic growth. Earth Planet. Sci. Lett. 268. 487–50.
Gebrande, H., TRANSALP Working Group, 2002. First deep seismic reflection images of the Eastern Alps reveal giant crustal wedges and transcrustal ramps. Geophys. Res. Lett. 29, 1452. https://doi.org/10.1029/2002GL0149.
Gerber, W., 2008. Evolution Tectono-Métamorphique du Briançonnais interne (Alpes Occidentales, massifs de Vanoise Sud et d'Ambin) : Comportement du socle et de sa couverture dans un contexte de Subduction Continentale Profonde. PhD Thesis. Univerité Pierre et Marie Curie, Paris, France.
Girault, J.B., Bellahsen, N., Boutoux, A., Rosenberg, C., Nanni, U., Verlaguet, A., Beyssac, O., 2020. The 3-D thermal structure of the Helvetic nappes of the European Alps: implications for collisional processes. Tectonics 39, e2018TC005334.
Girault, J.B., Bellahsen, N., Bernet, M., Pik, R., Loget, N., Lasseur, E., Rosenberg, C., Balvay, M., Sonnet, M., 2021. Exhumation of the Western Alpine collisional wedge: new thermochronological data. Tectonophysics. (in press).
Glotzbach, C., van der Beek, P.A., Spiegel, C., 2011. Episodic exhumation and relief growth in the Mont Blanc massif, Western Alps from numerical modelling of thermochronology data. Earth Planet. Sci. Lett. 304, 417–430.
Goffé, B., Bousquet, R., Henry, P., Le Pichon, X., 2003. Effect of the chemical composition of the crust on the metamorphic evolution of orogenic wedges. J. Metamorph. Geol. 21, 123–141.
Handy, M.R., Schmid, S.M., Bousquet, R., Kissling, E., Bernoulli, D., 2010. Reconciling plate-tectonic reconstructions of Alpine Tethys with with the geological–geophysical record of spreading and subduction in the Alps. Earth Sci. Rev. 102, 121–158.
Handy, M.R., Ustaszewski, K., Kissling, E., 2015. Reconstructing the Alps–Carpathians–Dinarides as a key to understanding switches in subduction polarity, slab gaps and surface motion. Int. J. Earth Sci. 104, 1–26. 10.1007/s00531-014-1060-3.
Herwegh, M., Berger, A., Wehrens, P., Baumberger, R., Kissling, E., 2017. Large-scale crustal-block-extrusion during late Alpine collision. Sci. Rep. 7. https://doi.org/10.1038/s41598-017-00440-0.
Herwegh, M., Berger, A., Glotzbach, C., Wangenheim, C., Mock, S., Wehrens, P., Baumberger, R., Egli, D., Kissling, E., 2020. Late stages of continent-continent collision: timing, kinematic evolution, and exhumation of the Northern rim (Aar Massif) of the Alps. Earth-Sci. Rev. 200, 102959. https://doi.org/10.1016/j.earscirev.2019.102959.
Hitz, L., 1995. The 3D crustal structure of the Alps of eastern Switzerland and western Austria interpreted from a network of deep-seismic profiles. Tectonophysics 248, 71–96.
Hoernes, S., Friedrichsen, H., 1974. Oxygen isotope studies on metamorphic rocks of the western Hohe Tauern area (Austria), Schweiz. Mineral. Petrogr. Mitt. 54, 769–788.
Hsu, K.J., 1979. Thin skinned plate tectonics during Neo-Alpine orogenesis. Am. J. Sci. 279, 353–366.
Hunziker, J.C., 1987. Radiogenic isotopes in very low grade metamorphism. In: Frey, M. (Ed.), Low Temperature Metamorphism. Blackie, Glasgow, pp. 200–226.
Jamieson, R.A., Beaumont, C., Fullsack, P., Lee, B., 1998. Barrovian regional metamorphism: Where's the heat?. In: Treloar, P.J., O'Brien, P.J. (Eds.), What Drives Metamorphism and Metamorphic Reactions?, 138. Geological Society, London, Special Publications, pp. 23–51.
Johnson, M.R.W., Harley, S.L., 2012. Orogenesis: The Making of Mountains. Cambridge University Press, p. 388.
Kirschner, D.L., Cosca, M., Masson, H., Hunziker, J.C., 1996. Staircase 40Ar/39Ar spectra of fine-grained white mica: timing and duration of deformation and empirical constraints on argon diffusion. Geology 24, 747–750.
Kissling, E., 2008. Deep structure and tectonics of the Valais- and the rest of the Alps. Bull. Angew. Geol. 13, 3–10.
Kummerow, J., Kind, R., Oncken, O., Giese, P., Ryberg, T., Wylegalla, K., Scherbaum, F., 2004. TRANSALP Working Group (2004). A natural and controlled source seismic profile through the Eastern Alps: TRANSALP. Earth Planet. Sci. Lett. 225, 115–129.
Laubscher, H.P., 1970. Bewegung und Wärme in der alpinen Orogenese. Schweiz. Mineral. Petrogr. Mitt. 5, 565–596.
Laubscher, H.P., 1988. Material balance in Alpine orogeny. Geol. Sot. Am. Bull. 100, 1313–1328.
Laubscher, H.P., 1991. The arc of the western Alps today. Eclogae Geol. Helv. 84 (631–659), 1991.
Le Breton, E., Handy, M.R., Molli, G., Ustaszewski, K., 2017. Post-20 Ma motion of the Adriatic plate: New constraints from surrounding Orogens and implications for crust-mantle decoupling. Tectonics 36. https://doi.org/10.1002/2016TC004443.
Le Breton, E., Brune, S., Ustaszewski, K., Zahirovic, S., Seton, M., Müller, R.D., 2021. Kinematics and extent of the Piemont–Liguria Basin – implications for subduction processes in the Alps. Solid Earth 12, 885–913. https://doi.org/10.5194/se-12-885-2021.
Lelarge, M.L., 1993. Thermochronologie par la méthode des traces de fission d'une marge passive (dôme de Ponta Grossa, SE Brésil) et au sein d'une chaîne de collision (zone externe de l'arc alpin, France). Université Joseph Fourier de Grenoble.
Liao, J., Gerya, T., Malusà, M., 2018. 3D modeling of crustal shortening influenced by along-strike lithological changes: implications for continental collision in the Western and Central Alps. Tectonophysics 746. https://doi.org/10.1016/j.tecto.2018.01.031.
Linzer, H.G., Decker, K., Peresson, H., Dell'Mour, R., Frisch, W., 2002. Balancing orogenic float of the Eastern Alps. Tectonophysics 354, 211–237.
Lippitsch, R., Kissling, E., Ansorge, J., 2003. Upper mantle structure beneath the Alpine orogen from high-resolution teleseismic tomography. J. Geophys. Res. 108, 2376.
Mair, D., Lechmann, A., Herwegh, M., Nibourel, L., Schlunegger, F., 2018. Linking Alpine deformation in the Aar Massif basement and its cover units: the case of the Jungfrau-Eiger mountains (Central Alps, Switzerland). Solid Earth 9, 1099–1122.
Malusà, M., Polino, R., Zattin, M., Bigazzi, G., Martin, S., Piana, F., 2005. Miocene to present differential exhumation in the Western Alps: Insights from fission track thermochronology. Tectonics 24, TC3004. https://doi.org/10.1029/2004TC001782.
Mancktelow, N.S., Pavlis, T.L., 1994. Fold-fault relationships in low-angle detachment systems. Tectonics 13, 668–685.
Métois, M., D'Agostino, N., Avallone, A., Chamot-Rooke, N., Rabaute, A., Duni, L., Kuka, K.R., Georgiev, I., 2015. Insights on continental collisional processes from GPS data: dynamics of the peri-Adriatic belts. J. Geophys. Res. Solid Earth 12, 8701–8871.
Milnes, G., 1978. Structural zones and continental collision, Central Alps. Tectonophysics 47, 369–392.
Mitterbauer, U., Behm, M., Brückl, E., Lippitsch, R., Guterch, A., Keller, G.R., Koslovskaya, E., Rumpfhuber, E.-M., Sumanovac, F., 2011. Shape and origin of the East-Alpine slab constrained by the ALPASS teleseismic model. Tectonophysics 510, 195–206.
Molli, G.-C., Crispini, L., Malusà, M., Mosca, P., Piana, F., Federico, L., 2010. Geology of the Western Alps-Northern Apennine junction area: a regional review. Journal of the Virtual Explorer, ISSN 1441–8142, volume 36. In: Beltrando, M., Peccerillo, A., Mattei, M., Conticelli, S., Doglioni, C. (Eds.), The Geology of Italy. p. 2010.
Moores, E., Twiss, R., 1995. Tectonics. W. H. Freeman, New York, p. 415.
Mugnier, J.L., Guellec, S., Ménard, G., Roure, F., Tardy, M., Vialon, P., 1990. A crustal scale balanced cross-section through the external Alps deduced front the ECORS profile. Mere. Soc. Geol. Fr. 170, 203–216.
Müller, W., Prosser, G., Mancktelow, N.S., Villa, I.M., Kelley, S., Viola, G., Oberli, F., Nemes, F., Neubauer, F., 2001. Geochronological constraints on the evolution of the Periadriatic Fault System (Alps). Int. J. Earth Sci. 90, 623–653.
Negro, F., Bousquet, R., Vils, F., Pellet, C.-M., Hänggi-Schaub, J., 2013. Thermal structure and metamorphic evolution of the Piemont-Ligurian metasediments in the northern Western Alps. Swiss J. Geosci. 106, 63–78.
Nibourel, L., Berger, A., Egli, D., Luensdorf, K., Herwegh, M., 2018. Large vertical displacements of a crystalline massif recorded by Raman thermometry. Geology 46, 879–882.
Nicolas, A., Hirn, A., Nicolich, R., Polino, R., 1990. Lithospheric wedging in the western Alps inferred from the ECORS-CROP traverse. Geology 18, 587–590.
Niggli, E., 1970. Alpine Metamorphose und alpine Gebirgsbildung. Fortschr. Mineral. 47, 16–26.
Niggli, E., 1986. Notizen zur Geschichte der Erforschung der Metamorphosen in den Zentralalpen. Schweiz. Mineral. Petrogr. Mitt. 66, 5–11.
Niggli, E., et al., 1978. Metamorphic map of the Alps 1:1.000.000 and Explanatory text. In: Subcomm. Cartography of Metamorphic Belts of the World. Unesco Paris, Leiden, p. 242.
Nussbaum, C., 2000. Neogene tectonics and thermal maturity of sediments of the easternmost Southern Alps (Friuli area, Italy). PhD Thesis. Univ. of Neuchâtel, Switzerland.
Oberli, F., Meier, M., Berger, A., Rosenberg, C.L., Gieré, R., 2004. U-Th-Pb and 230Th/238U disequilibrium isotope systematics: Precise accessory mineral chronology and melt evolution tracing in the Alpine Bergell intrusion. Geochim. Cosmochim. Acta 68, 2543–2560. https://doi.org/10.1016/j.gca.2003.10.017.
Ortner, H., 2006. Kinematics of the Inntal shear zone–sub-Tauern ramp fault system and the interpretation of the TRANSALP seismic section, Eastern Alps, Austria. Tectonophysics 414, 241–258.
Ortner, H., Aichholzer, S., Zerlauth, M., Pilser, R., Fügenschuh, B., 2015. Geometry, amount, and sequence of thrusting in the Subalpine Molasse of western Austria and southern Germany, European Alps. Tectonics 34, 1–30.
Oxburgh, E.R., Turcotte, D.L., 1974. Thermal gradients and regional metamorphism in overthrust terrains with special reference to the Eastern Alps. Schweiz. Mineral. Petrogr. Mitt. 543, 641–662.
Pfiffner, O.A., 2011. Structural Map of the Helvetic Zone of the Swiss Alps, Including Vorarlberg (Austria) and Haute Savoie (France), 1: 100 000. Geological Special Map *128*. Explanatory notes. Federal Office of Topography swisstopo, p. 128.
Pfiffner, O.A., 2014. Geology of the Alps. John Wiley & Sons, New York, USA.
Pieri, M., Groppi, G., 1981. Subsurface geological structure of the Po Plain, Italy. In: Consiglio Nazionale di Richercha, Progetto Finalizzato Geodinamica, 414. p. 13.
Platt, J.P., 1984. Balanced cross-sections and their implications for the deep structure of the Northwest Alps: discussion. J. Struct. Geol. 6, 603–606.
Pomella, H., Ortner, H., Zerlauth, M., Fügenschuh, B., 2015. The Alpine nappe stack in western Austria: a crustal-scale cross-section. Int. J. Earth Sci. 104, 733–745. https://doi.org/10.1007/s00531-014-1097-3.
Ratschbacher, L., Frisch, W., Linzer, H.-G., 1991. Lateral extrusion in the Eastern Alps: part II. Structural analysis. Tectonics 10, 257–271.
Ridley, J., 1989. Vertical movement in orogenic belts and the timing of metamorphism relative to deformation. In: Daly, J.S., Cliff, R.A., Yardley, B.W.D. (Eds.), Evolution of Metamorphic Belts, 43. Geological Society Special Publication, pp. 103–116.
Robl, J., Stüwe, K., 2005. Continental collision with finite indenter strength 2: European Eastern Alps. Tectonics 24.
Roeder, D., 1989. South Alpine thrusting and trans-Alpine convergence. Geol. Soc. Spec. Publ. 45, 211–227.
Rolland, Y., 2014. Collision kinematics in the Western Alps. Tectonics 33, 1055–1088. https://doi.org/10.1002/2013TC003453.
Rolland, Y., Cox, S., Bouiller, A.-M., Pennacchioni, G., Mancktelow, N.S., 2003. Rare earth

and trace element mobility in mid-crustal shearzones: insights from the Mont Blanc Massif (Western Alps). Earth Planet. Sci. Lett. 214, 203–219.
Rolland, Y., Rossi, M., Cox, S.F., Corsini, M., Mancktelow, N., Pennacchioni, G., Boullier, A.M., 2008. 40Ar/39Ar dating of synkinematic white mica: insights from fluid-rock reaction in low-grade shear zones (Mont Blanc Massif) and constraints on timing of deformation in the NW external Alps. Geol. Soc. Lond., Spec. Publ. 299, 293–315.
Romer, R.L., Schärer, U., Steck, A., 1996. Alpine and pre-Alpine magmatism in the root-zone of the Western Central Alps. Contrib. Mineral. Petrol. 123, 138–158.
Rosenberg, C.L., Kissling, E., 2013. Three-dimensional insight into Central-Alpine collision: Lower-plate or upper-plate indentation?. Geology 41, 1219–1222.
Rosenberg, C.L., Berger, A., Bellahsen, N., Bousquet, R., 2015. Relating orogen-width to shortening, erosion, and exhumation during Alpine collision. Tectonics 34, 1306–1328.
Rosenberg, C., Schneider, S., Scharf, A., Bertrand, A., Hammerschmidt, K., Rabaute, A., Brun, J.P., 2018. Relating collisional kinematics to exhumation processes in the Eastern Alps. Earth Sci. Rev. 176, 311–344.
Roure, F., Polino, R., Nicolich, R., 1990a. Poinçonnement, rétrocharriages et chevauchements post-basculement dans les Alpes occidentales : évolution intracontinentale d'une chaîne de collision. C. R. Acad. Sci. Paris, t. 309, 283–290. Série II.
Roure, F., Polino, R., Nicolich, R., 1990b. Early Neogene deformation beneath the Po plain, constraints on the post-collisional Alpine evolution. In: Roure, F. (Ed.), et al., Deep Structure of the Alps, 156. pp. 309–322. Mem. Soc. Geo/. Fr.
Rubatto, D., Hermann, J., Berger, A., Engi, M., 2009. Protracted fluid-induced melting during Barrovian metamorphism in the Central Alps. Contrib. Mineral. Petrol. 158, 703–722.
Sanchez, G., Rolland, Y., Schneider, J., Corsini, M., Oliot, E., Goncalves, P., Verati, C., Lardeaux, J.-M., Marquer, D., 2011. Dating low-temperature deformation by 40Ar/39Ar on white mica, insights from the Argentera-Mercantour Massif (SW Alps). Lithos. https://doi.org/10.1016/j.lithos.2011.03.009.
Schmid, S.M., 1975. The glarus overthrust: field evidence and mechanical model. Eclogae Geol. Helv. 68, 247–280.
Schmid, S.M., Froitzheim, N., 1993. Oblique slip and block rotation along the Engadine line. Eclogae Geol. Helv. 86, 569–593.
Schmid, S.M., Kissling, E., 2000. The arc of the Western Alps in the light of geophysical data on deep crustal structure. Tectonics 19, 62–85. https://doi.org/10.1029/1999TC900057.
Schmid, S., Pfiffner, O.A., Froitzheim, N., Schönborn, G., Kissling, E., 1996. Geophysical-geological transect and tectonic evolution of the Swiss-Italian Alps. Tectonics 15, 1036–1064. https://doi.org/10.1029/96TC00433.
Schmid, S.M., Fügenschuh, B., Kissling, E., Schuster, R., 2004. Tectonic map and overall architecture of the Alpine orogen. Eclogae Geol. Helv. 97, 93–117. https://doi.org/10.1007/s00015-004-1113-x.
Schmid, S.M., Scharf, A., Handy, M.R., Rosenberg, C.L., 2013. The Tauern Window (Eastern Alps, Austria): a new tectonic map, with cross sections and a tectono-metamorphic synthesis. Swiss J. Geosci. 106, 1–32.
Schmid, S.M., Kissling, E., Diehl, T., van Hinsbergen, D.J., Molli, G., 2017. Ivrea mantle wedge, arc of the Western Alps, and kinematic evolution of the Alps-Apennines orogenic system. Swiss J. Geosci. 110, 581–612.
Schönborn, G., 1992. Alpine tectonics and kinematic models of the central Southern Alps. Mem. Sci. Geol. Padova 44, 229–293.
Schönborn, G., 1999. Balancing cross-sections with kinematic constraints: the dolomites (northern Italy). Tectonics 18, 527–545.
Schwartz, S., Lardeaux, J.M., Tricart, P., Guillot, S., Labrin, E., 2007. Diachronous exhumation of HP–LT metamorphic rocks from South-Western Alps: evidence from fission-track analysis. Terra Nova 19, 133–140.
Selverstone, J., 1988. Evidence for east–west crustal extension in the Eastern Alps: implications for the unroofing history of the Tauern Window. Tectonics 7, 87–105.
Selverstone, J., 1993. Micro- to macroscale interactions between deformational and metamorphic processes, Tauern Window, Eastern Alps. Schweiz. Mineral. Petrogr. Mitt. 73, 229–239.
Seward, D., Mancktelow, N.S., 1994. Neogene kinematics of the central and western Alps : evidence from fission-track dating. Geology 22, 803–806.
Simoes, M., Avouac, J.-P., Beyssac, O., Goffé, B., Farley, K.A., Chen, Y.G., 2007. Mountain building in Taiwan: a thermokinematic model. J. Geophys. Res. 112, B11405. https://doi.org/10.1029/2006JB004824.
Sissingh, W., 1997. Tectonostratigraphy of the North Alpine Foreland Basin: correlation of Tertiary depositional cycles and orogenic phases. Tectonophysics 282, 223–256.
Spillmann, P., 1993. Die Geologie des penninisch-ostalpinen Grenzbereichs im südlichen Berninagebirge, PhD, ETH Zürich, Nr. 10175.
Stampfli, G., 1993. Le Briançonnais, terrain exotique dans les Alpes?. Eclogae Geol. Helv. 86, 1–45.
Stipp, M., Stünitz, H., Heilbronner, R., Schmid, S.M., 2002. The eastern Tonale fault zone: a 'natural laboratory' for crystal plastic deformation of quartz over a temperature range from 250 to 700 8C. J. Struct. Geol. 24, 1861–1884.
Stüwe, K., Sandiford, M., 1995. Mantle-lithospheric deformation and crustal metamorphism with some speculations on the thermal and mechanical significance of the Tauern event, Eastern Alps. Tectonophysics 242, 115–132.
Stüwe, K., Schuster, R., 2010. Initiation of subduction in the Alps: continent or ocean?. Geology 38, 175–178. https://doi.org/10.1130/G30528.1.
Tardy, M., Deville, E., Fudral, S., Guellec, S., Ménard, G., Thouvenot, F., Viallon, P., 1990. Interprétation structural des données de sismique réflexion profonde Ecors Crop Alpes entre le Front Pennique et la Ligne du Canavese (Alpes occidentales). Mém. Soc. Géol France 156, 217–226.
Tricart, P., Schwartz, S., 2006. A north-south section across the Queyras Schistes lustrés (Piedmont zone,Western Alps): syn-collision refolding of a subduction wedge. Eclogae Geol. Helv. 99, 429–442.
Twiss, R.J., Moores, E.M., 1992. Structural Geology. W.H. Freeman, New York, NY, p. 1992. ISBN: 9780716722526.
Ustaszewski, K., Schmid, S.M., Fügenschuh, B., Tischler, M., Kissling, E., Spakman, W., 2008. A map-view restoration of the Alpine-Carpathian-Dinaridic system for the early Miocene. Swiss J. Geosci. 101, 273–294.
van der Beek, P.A., Valla, P.G., Herman, F., Braun, J., Persano, C., Dobson, K.J., Labrin, E., 2010. Inversion of thermochronological age–elevation profiles to extract independent estimates of denudation and relief history — II : Application to the French Western Alps. Earth Planet. Sci. Lett. 296, 9–22.
van Hinsbergen, D.J.J., Torsvik, T.H., Schmid, S.M., Matenco, L.C., Maffione, M., Vissers, R.L.M., Gürer, D., Spakman, W., 2020. Orogenic architecture of the Mediterranean region and kinematic reconstruction of its tectonic evolution since the Triassic. Gondwana Res. 81, 79–229.
Vance, J.A., 1999. Zircon fission track evidence for a Jurassic (Tethyan) thermal event in the Western Alps. In: Martin, S., Polino, R. (Eds.), Fission track Analysis: Theory and applications. Mem. Sci. Geol., Padova, 51. pp. 473–476.
Vilà, M., Fernández, M., Jiménez-Munt, I., 2010. Radiogenic heat production variability of some common lithological groups and its significance to lithospheric thermal modeling. Tectonophysics 490, 152–164.
von Eynatten, H., Schlunegger, F., Gaupp, R., Wijbrans, J.R., 1999. Exhumation of the Central Alps: evidence from 40Ar/39Ar laserprobe dating of detrital white mica from the Swiss Molasse Basin. Terra Nova 11, 284–289.
Ward, S.N., 1994. Constraints in the seismotectonics of the Central Mediterranean from very long baseline interferometry. Geophys. J. Int. 117, 441–452.
Wenk, E., 1975. Zur alpinen Metamorphose. Schweiz. Mineral. Petrogr. Mitt. 55, 116–125.
Westaway, R., 1990. The Tripoli, Libya, earthquake of September 4, 1974: Implications for the active tectonics of the Central Mediterranean. Tectonics 9, 231–248.
Wiederkehr, M., Bousquet, R., Ziemann, M.A., Berger, A., Schmid, S.M., 2011. 3-D assessment of peak-metamorphic conditions by Raman spectroscopy of carbonaceous material: an example from the margin of the Lepontine dome (Swiss Central Alps). Int. J. Earth Sci. 100, 1029–1063.
Willett, S.D., Brandon, M.T., 2002. On steady state in mountain belts. Geology 30, 175–178.
Willett, S., Beaumont, C., Fullsack, P., 1993. Mechanical model for the tectonics of doubly vergent compressional orogens. Geology 21, 371–374.
Wolff, R., Dunkl, I., Kiesselbach, G., Wemmer, K., Siegesmund, S., 2012. Thermochronological constraints on the multiphase exhumation history of the Ivrea-Verbano Zone of the Southern Alps. Tectonophysics 579, 104–117.
Zanoni, D., Spalla, I.M., Gosso, G., Zucali, M., 2008. Plutoni tardo-collisionali nella crosta profonda esumata della Zona Sesia Lanzo: implicazioni per la geodinamica delle Alpi Occidentali Interne. Rend. SGI, Note Brevi 1, 199–202.
Zhao, L., Paul, A., Guillot, S., Solarino, S., Malusà, M.G., Zheng, T., Aubert, C., Salimbeni, S., Dumont, T., Schwartz, S., 2015. First seismic evidence for continental subduction beneath the Western Alps. Geology 43, 815–818.